NUREG/CR--4693

TI87 003446

NUREG/CR-4693
SAND86-1598
RW

ASSESSMENT OF RADIONUCLIDE VAPOR-PHASE TRANSPORT IN UNSATURATED TUFF

Douglas M. Smith[1]
C. David Updegraff[2]
Evaristo J. Bonano
and
John D. Randall[3]

November 1986

Sandia National Laboratories
Albuquerque, NM 87185
Operated by
Sandia Corporation
for the
Department of Energy

Prepared for
Division of Engineering Safety
Office of Nuclear Regulatory Research
U.S. Nuclear Regulatory Commission
Washington, DC 20555
Under Memorandum of Understanding DOE 40-550-75
NRC FIN No. A-1266

---

[1] University of New Mexico, Albuquerque, NM
[2] Science Applications International Corporation, Albuquerque, NM
[3] U.S. Nuclear Regulatory Commission, Washington, DC

E&B

DISCLAIMER

DISCLAIMER

Portions of this document may be illegible in electronic image products. Images are produced from the best available original document.

ABSTRACT

This report describes bounding calculations performed to investigate the possibility of radionuclide migration in a vapor phase associated with the emplacement of high-level waste canister in unsaturated tuff formations. Two potential radionuclide transport mechanisms in the vapor phase were examined: aerosol migration and convection/diffusion of volatile species. The former may have significant impact on the release of radionuclides to the accessible environment as the concentration in the aerosols will be equal to that in the ground water. A conservative analysis of air diffusion in a stagnant liquid film indicated that for all expected repository conditions, aerosol formation is not possible. The migration of volatile species was examined both in the vicinity of a waste canister and outside the thermally disturbed zone. Two-dimensional (radial) and three-dimensional (radial-vertical) coupled heat transfer-gas flow-liquid flow simulations were performed using the TOUGH computer code. The gas flow rate relative to the liquid flow rate predicted from the simulations allowed calculations of mobility ratios due to convection which led to the conclusion that, except for the immediate region near the canister, transport in the liquid phase will be dominant for radionuclides heavier than radon. Near the waste canister, iodine transport may also be important in the vapor phase. Bounding calculations for vertical mobility ratios were carried out as a function of saturation. These calculations are conservative and agree well with the two-dimensional simulations. Based on this analysis, it is clear that vapor-phase transport will not be important for radionuclides such as cesium and heavier species. Vapor transport for iodine may play a role in the overall release scenario depending on the particular repository conditions.

TABLE OF CONTENTS

LIST OF FIGURES

LIST OF TABLES

1. INTRODUCTION

To date, little work has been reported on the potential of radionuclide transport in the vapor phase when a high-level waste canister is emplaced in unsaturated tuff. Vapor-phase radionuclide transport may occur via two different pathways. Aerosols may form as the temperature, and hence, air solubility in the ground water change [Green and Evans, 1983]. These aerosols would contain radionuclide concentrations equivalent to the ground water and not be limited to the volatility of the species. Radionuclides may also be transported in the vapor phase via convection and diffusion/dispersion if the species are sufficiently volatile. The degree of volatility necessary for significant release via this mode depends upon the relative velocities of the two phases, the tuff liquid saturation, vapor- and liquid-phase retardation factors, and the distribution coefficient for the radionuclide between the vapor and liquid phases.

The effects of unsaturated media versus saturated media on radionuclide transport are two-fold. Depending on how the ground water wets the porous solid, radionuclides in the liquid phase may not have access to all adsorption sites. This implies that the retardation factor for the liquid phase will vary with saturation. The complex functional relationship between retardation and saturation will depend on variables including the radionuclide, ground-water chemistry, retardation mechanism, pore/fracture shape and size distribution, and temperature. In addition, if the radionuclides are sufficiently volatile, transport may occur in the vapor phase. Vapor-phase transport may be the result of convection and/or diffusion. Retardation of radionuclides in the vapor phase will depend upon partitioning between the gas and liquid phases as well as adsorption sites which are directly available to the vapor phase (i.e., where the surface is not wetted). For fractured media, different transport mechanisms may be important for the fractures and matrix. In this report, we will outline a preliminary "order of magnitude" analysis to provide an assessment of which transport mechanisms (i.e., convection, bulk diffusion, thermal diffusion, etc.) may be important in order to assess the possible role of vapor-phase transport. The effect of changing saturation on radionuclide transport in the liquid phase will not be addressed in this report.

In this work, we attempt to identify vapor-phase release pathways for radionuclide migration which may be significant, as compared to liquid-phase release pathways, for expected repository conditions. Since aerosol formation and subsequent migration could potentially lead to large release rates, we have explored the possibility of aerosol formation for a wide range of repository conditions. To study convection and/or diffusion in both the liquid and vapor phases requires a solution of the coupled flow-heat transfer problem surrounding a waste canister in a repository. From this solution, spatial and temporal profiles of gas and liquid velocity, saturation, and temperature may be obtained. Since gas and/or liquid velocities may be very small, the mass-transfer Peclet

number can be calculated for each phase in order to ascertain the relative importance of convection and diffusion for both the liquid and vapor phases. If convection is the primary transport mode for both phases or if diffusion is the dominant mode for both phases, simple mobility ratios may be defined which yield a first-order approximation concerning the relative importance of transport in the vapor phase.

2. AEROSOL TRANSPORT

2.1 Aerosol Formation - Background

Recent concern has been raised about the possibility of radionuclide transport in the vapor phase within fractures as an aerosol (i.e., very small droplets in the size range of 0.1 to 10 μm) by Green and Evans [1983]. This transport mode is of particular concern since the concentration of radionuclides in the aerosol will be equal to the liquid phase concentration and not be limited by vapor-liquid equilibrium. This could result in effective vapor phase concentrations which are several orders of magnitude higher than the equilibrium value. Although the diffusive transport of aerosols, via Brownian motion, will be a very slow process, convective transport could result in a relatively high radionuclide release rate since the velocity of the aerosols will be on the same order as the bulk velocity of the vapor.

It has been demonstrated by Tomaides and Whitby [1976] that the bursting of gas bubbles at a gas-liquid interface will result in the production of an aerosol if the gas bubbles are sufficiently energetic. In that work, aerosol particles in the size range of 1-100 μm were produced from the collapse of 1.4 and 5.5 mm bubbles. The bubbles were produced by forcing air through a jet located at the bottom of a fluid column. After bubble detachment from the jet, the bubble is accelerated through the column by buoyancy forces. As the air bubble reaches the surface of the fluid, the bubble collapses and ejects aerosols into the air. In order to produce sufficient bubble velocities for aerosol formation, a column height of ≈10 cm was used.

The formation of aerosols from the liquid phase contained on the fracture wall in unsaturated tuff is visualized to be a multiple step process. These steps are:

1) Ground water at ambient temperatures migrates towards the waste canister, is heated/vaporized and the vapor flows away from the canister. This is the result of the so-called "heat pipe" effect.

2) The solubility of the air components (i.e., oxygen, nitrogen) in the ground water decreases with increasing temperature.

3) Air components migrate via diffusion/convection through the liquid film to the gas-liquid interface.

4) Air components desorb from the interface into the bulk gas/vapor phase.

5) If the air transport rate is not sufficiently high, the ground water will become supersaturated.

6) If the degree of supersaturation is high, gas bubble formation (nucleation) will occur.

7) Air bubbles will migrate to the surface of the liquid ground-water film if the film thickness is large as compared to the air bubble size.

8) If the bubble velocity is large, the bubble will collapse such that aerosols are produced.

From the known dynamics of heat and fluid transfer in the near-field for unsaturated repository sites [Tien, et.al., 1985], steps 1 through 4 in the aerosol formation scenario, discussed previously, will occur given sufficient heat loadings, etc.. However, for aerosol formation to occur, steps 5 through 8 must all occur. If the conditions for any one of these steps is not met, then aerosol transport may be safely neglected.

A necessary prerequisite for the existence of aerosols in the unsaturated portions of tuff is the formation of air bubbles in the liquid phase. If it can be demonstrated that air bubbles will not form for any probable set of repository conditions, then the concept of radionuclide migration via aerosol transport in the vapor phase may be neglected. Whether air bubbles will form in the liquid phase as the liquid and vapor temperature change will depend upon the degree of air supersaturation which exists in the ground water. As a result of surface tension forces, the pressure in an air bubble and the liquid are not the same. This pressure differential is given by:

$$P_b - P_l = 2\,\sigma/r_b \qquad (1)$$

where P_b is the air bubble pressure, P_l is the liquid pressure, σ is the surface tension and r_b is the bubble radius. Therefore, for a bubble to form, the air concentration must be above its solubility limit (i.e. supersaturated). The degree of supersaturation required to obtain bubble formation is a complex function of numerous variables including the type and number of nucleation sites, ground-water impurities, pressure and temperature. By analogy to nucleate boiling, the minimum supersaturation necessary for bubble formation is $\approx$2% when conditions are most favorable for bubble formation [Hsu and Graham, 1976]. It is not clear if adequate film thickness exists for gas bubbles, if they do actually form, to be accelerated to sufficient velocities for aerosol generation in tuff fractures. The fracture width for six tuff samples has been found to range between 57 and 252 μm [Ogard et al., 1983]. This implies that the maximum possible liquid film thickness would on the order of 100 μm. Also, for air bubbles to exist in such a thin film, the degree of air supersaturation must be substantially higher to offset the larger ΔP across the bubble interface as given by Equation (1). It is unlikely, given this narrow film thickness, that bubble velocities would reach large enough values to result in a sufficiently high Weber number for aerosol formation [Hidy, 1984].

To ascertain whether aerosol transport will occur or not for all possible repository conditions, an analysis that indicates that any of steps 5

through 8 will not occur is sufficient. Since diffusion in a stagnant film is the best understood of the transport processes, in steps 5 through 8, we will perform a conservative analysis of air diffusional transport in a stagnant liquid film to determine the degree of supersaturation. If the air transport rate in the ground water is high such that a significant degree of supersaturation does not occur, there is no point in analyzing additional transport steps. If large supersaturation does occur, this does not imply aerosol formation will occur but that other transport steps must be studied.

2.2 Aerosol Formation - Model

We consider a liquid film of thickness, L, on a fracture wall which has an initial air concentration, C_0. Since the longitudinal and lateral dimensions of fractures in tuff are usually much greater than the fracture width, the problem may be treated in one dimension only. For simplicity, the transport properties of oxygen and nitrogen are assumed to be similar enough that we may treat the mixture as a single component using averaged properties. At some time zero, the temperature of the liquid and vapor phases begins to increase. This may be the result of the film moving closer to the container and/or the temperature field extending farther into the repository as a function of time. After sufficient time, the temperature of the tuff approaches a constant value with the associated air solubility in the film being, C_f. The rate at which the temperature increases over this period of time is a function of numerous variables which we do not consider in this work. Instead, we assume that the equilibrium solubility of air in the liquid film decreases exponentially from C_0 to C_f. The time constant for this exponential decay is t_d. Although one would not expect such a straightforward relationship to describe the actual time/temperature/solubility response, the sensitivity of our analysis to the shape of this response is expected to be low.

As the temperature of the liquid film changes, air will be transported from the liquid film, across the gas-liquid interface and to the bulk gas phase. This transport will occur via a combination of mechanisms. These include:

1) Bulk diffusion of air in water as a result of concentration gradient.

2) Thermal diffusion resulting from the large thermal gradients in the near-field region.

3) Forced convection arising from the bulk flow components of both the liquid and gas/vapor phases.

4) Free convection due to temperature gradients in the film.

In order to perform the most conservative analysis, we will assume that

only bulk diffusion is serving to transport air through the film to the gas/vapor-liquid interface. The contributions of mechanisms 2 through 4 will only serve to increase the total transport rate. If the bulk diffusion coefficient for air in water is assumed to be independent of temperature, the governing equation for the air concentration in the film and associated boundary/initial conditions are given by:

$$D_{AB}\,\partial^2 C/\partial x^2 = \partial C/\partial t \qquad (2)$$

and

$$C(x,0) = C_o, \qquad \partial C/\partial x(0,t) = 0,$$

$$C(L,t) = (C_o - C_f)\exp(-t/t_d) + C_f$$

These boundary conditions correspond to no-flux at the fracture-wall/liquid-film interface (x=0) and vapor-liquid equilibrium at the vapor-liquid interface (x=L). Rewriting Equation (2) in nondimensional form:

$$\partial^2\Theta/\partial\eta^2 = \partial\Theta/\partial\tau \qquad (3)$$

and

$$\Theta(\eta,0) = 0, \qquad \partial\Theta/\partial\eta(0,\tau) = 0,$$

$$\Theta(1,\tau) = (1-\beta)\exp(-t^*\tau) - (1-\beta)$$

where Θ is $(C-C_o)/C_o$, β is C_f/C_o and η is x/L. The dimensionless time, τ, is defined as $D_{AB}t/L^2$ and t^* is $L^2/t_d D_{AB}$. The dimensionless group, t^*, is a measure of the relative timescales of air concentration change due to the changing air solubility and diffusion. Equation (3) may be reduced to an ordinary differential equation via application of the following finite Fourier transform [Ozisik, 1968]:

$$\bar{\Theta}(\lambda_n,\tau) = \sqrt{2}\int_0^1 \Theta(\eta,\tau)\cos(\lambda_n,\eta)d\eta \qquad (4)$$

The solution, Θ, is obtained from $\bar{\Theta}$ by applying the inversion:

$$\Theta(\eta,\tau) = \sqrt{2}\sum_{n=0}^{\infty} \cos(\lambda_n,\eta)\,\bar{\Theta}(\lambda_n,\tau) \qquad (5)$$

where the eigenvalues, λ_n, are $(2n+1)\pi/2$. From the application of the transform/inversion pair given by Equations (4) and (5), an expression for the spatial and temporal variation of Θ is obtained:

$$\Theta(\eta,\tau) = 2(1-\beta) \sum_{n=0}^{\infty} (-1)^n \lambda_n \cos(\lambda_n \eta)$$

$$\left\{[\exp(-t^*\tau) - \exp(-\lambda_n^2\tau)]/(\lambda_n^2 - t^*) - [1 - \exp(-\lambda_n^2\tau)]/\lambda_n^2\right\} \quad (6)$$

The point of maximum supersaturation in the film at any time will always occur at the fracture wall-film interface. Therefore, the fractional degree of maximum supersaturation, S', may be defined as:

$$S'(\tau) = C(0,\tau)/C(1,\tau) - 1 \quad (7)$$

Combining Equations (6) and (7), an expression for $S'(\tau)$ in terms of the three dimensionless parameters, τ, β and t^* is obtained.

$S'(\tau) =$

$$\left\{ \frac{1 + 2(1-\beta) \sum_{n=0}^{\infty} (-1)^n \lambda_n \left[\frac{(\exp(-t^*\tau) - \exp(-\lambda_n^2\tau)}{(\lambda_n^2 - t^*)} - \frac{(1 - \exp(-\lambda_n^2\tau)}{\lambda_n^2} \right]}{(1-\beta \exp(-t^*\tau) + \beta} \right\} - 1 \quad (8)$$

Equation (8) may be evaluated to calculate S', and hence determine the range of conditions when air bubbles will form. We should note that the infinite series contained in Equation (8) converges very slowly at small dimensionless times. In order to retain sufficient accuracy in S', the expansion included 10,000 terms. For the purpose of completion, we would like to mention that a short time asymptotic solution can be obtained which is not plagued by lack of convergence. This solution is presented in the Appendix. Equation (8) has been evaluated for various values of β, t^* and τ using a Vax 11/7895 computer with double precision arithmetic.

2.3 Aerosol Formation - Results

The variation of the degree of supersaturation has been calculated as a function of time for various values of the groups D_{AB}/L^2 and t_d. The value of β, the ratio of final solubility to initial solubility, was held constant at 0.5. This β value is typical of minimum and maximum solubilities associated with the temperatures expected near a canister. Since S' is only a weak function of β, we will not report results obtained using other β values. Figure 2.1 contains plots of the percent

supersaturation, 100 S', as a function of time for a decay constant associated with the solubility concentration change of 100 years (i.e. 63.2% of the change in solubility has occurred after 100 years). The value of the diffusion group, D_{AB}/L^2, is varied between 10^{-8} and 10^{-11} sec^{-1}. Very small values of D_{AB}/L^2(i.e. 10^{-11})correspond to no transfer of dissolved air from the liquid film to the gas-liquid interface. The continuous increase in supersaturation occurs from the changing film-gas interface concentration and a constant concentration at the wall-liquid interface. As D_{AB}/L^2 is increased, diffusional transport serves to decrease the degree of supersaturation. For values of 10^{-8} and greater, no gas bubble formation will occur. We should note that the curves above the bubble limit, 2% supersaturation, overpredict the degree of supersaturation since the formation of air bubbles would serve to decrease the concentration of air in the film. Since we are only trying to determine under what repository conditions bubble formation will occur, we have not attempted to determine the transport rate of dissolved air as bubbles through the liquid film.

Figure 2.2 is similar to the preceding plot except that the value of t_d is 0.1 years. This is a very conservative value of t_d which is an upper bound on the near-field ground-water velocity. Figure 2.2 is the same as Figure 2.1 except that the corresponding D_{AB}/L_2 values and overall timescales are different. This figure serves to illustrate that only the ratio of the timescales for air diffusion to the gas-liquid interface and the total air solubility change is important.

Applying our calculations to actual repository conditions requires an estimate of the magnitude of D_{AB}/L^2 for unsaturated tuff. The value of D_{AB} for dissolved oxygen/nitrogen in water for the temperature range of interest is on the order of 2×10^{-9} to 1×10^{-8} m^2/s [see Satterfield, 1970 or Danckwerts, 1970]. Based upon the fracture thickness described earlier, L could be expected to vary between 1 and 100 μm. Therefore, the value of D_{AB}/L^2 for unsaturated tuff will range between 0.2 and 10,000. In other words, the diffusion process would have to be at least 7 orders of magnitude less before gas bubble formation can even be considered if the solubility change occurs over a time span of 100 years. Since the ratio of the timescales for diffusion and solubility concentration change is the important parameter with regard to the possibility of bubble formation, the limiting values of D_{AB}/L^2 for other values of t_d are directly determined from this result. If the characteristic time for the solubility change is 1 year, then the diffusion rate would have to be at least 5 orders of magnitude less. Based upon the results of our analysis of air diffusion in the liquid film, it is reasonable and conservative to say that gas bubbles, and hence aerosols, will not form under expected repository conditions. We should note that conservative assumptions have been made throughout this analysis. For example, the assumption that the liquid film is stagnant and air transport is by molecular diffusion only is certainly not valid under near-field repository conditions. However, the presence of temperature variations and local turbulence will certainly

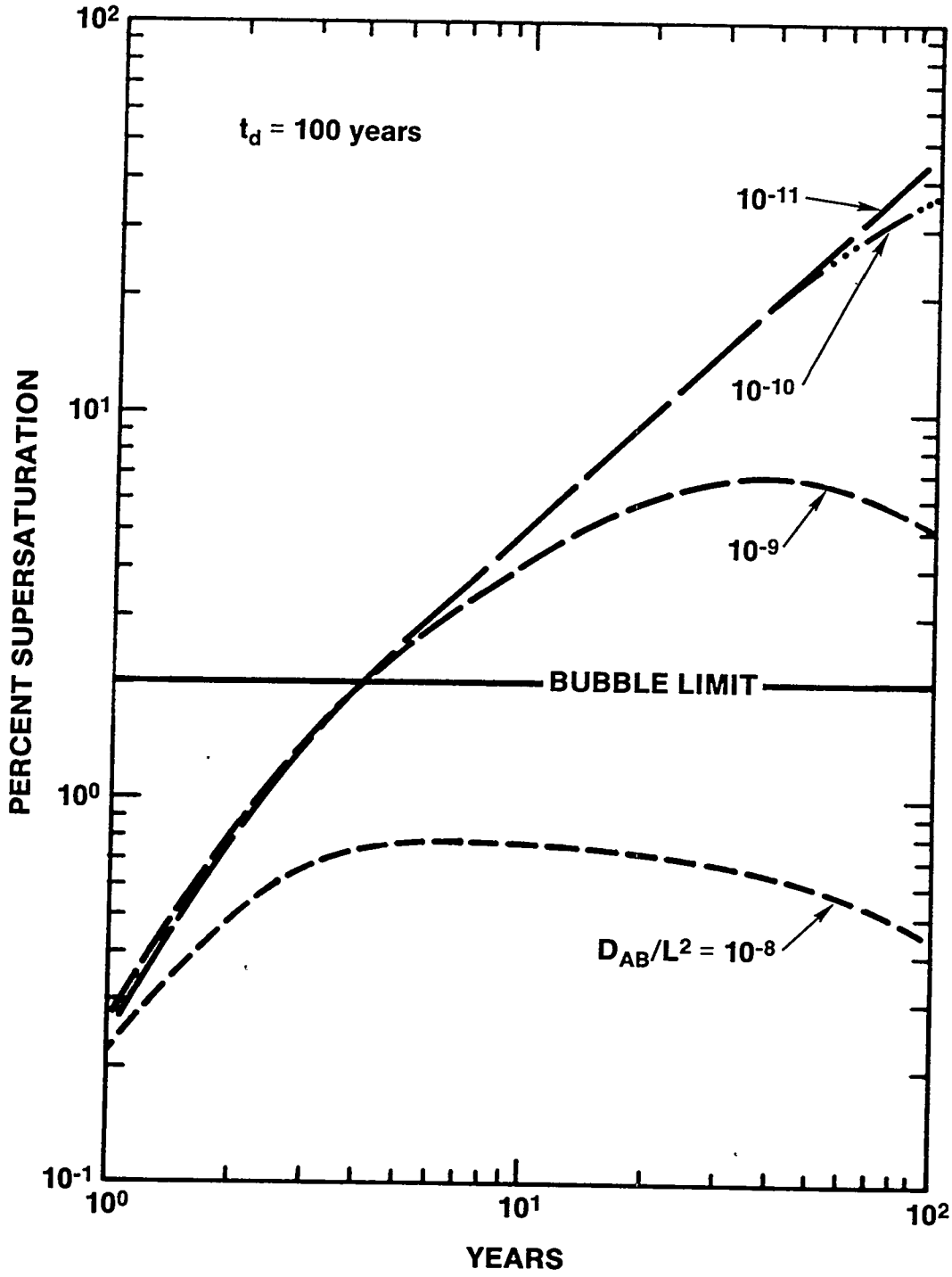

Figure 2.1 Variation of Air Supersaturation as a Function of Time and D_{AB}/L^2, t_d = 100 Years.

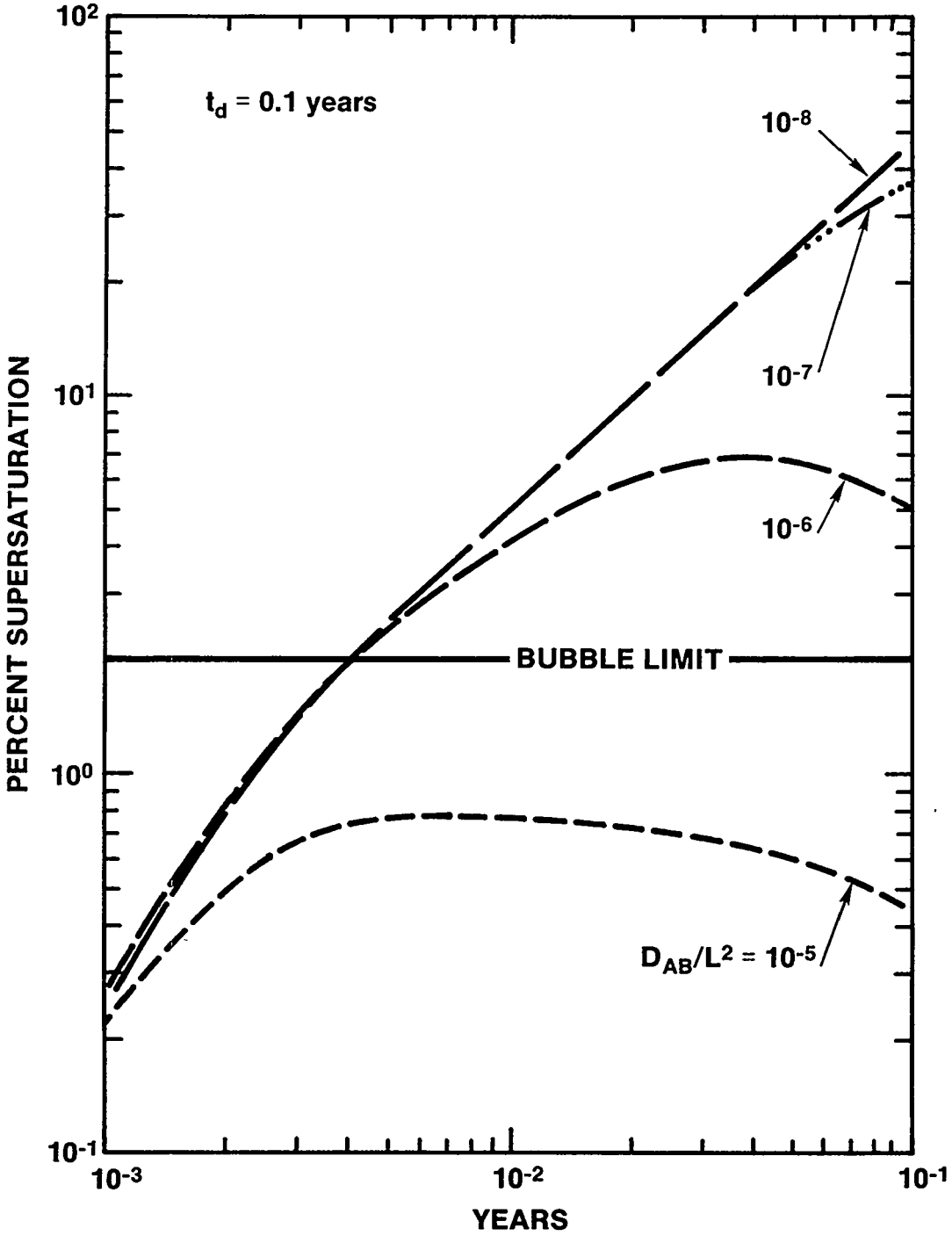

Figure 2.2 Variation of Air Supersaturation as a Function of Time and D_{AB}/L^2, t_d = 0.1 Years.

serve to increase the air transport rate and hence, decrease supersaturation as compared to our prediction.

2.4 Aerosol Transport - Conclusions

Based upon an analysis of the various steps necessary in an aerosol formation scenario, we have identified a straightforward set of calculations to address the possibility of aerosol transport in the unsaturated zone. Based upon a suite of calculations which cover the range of possible repository conditions, it is clear that aerosol formation will not occur and the concept of radionuclide transport as an aerosol may be safely neglected.

3. VAPOR PHASE FLOW/DIFFUSION

3.1 Flow/Diffusion Background

The effects of unsaturated media versus saturated media on radionuclide transport are twofold. Depending on how the ground water wets the porous solid, radionuclides in the liquid phase may not have access to all adsorption sites. This implies that the retardation factor for the liquid phase will vary with saturation. The complex functional relationship between retardation and saturation will depend on variables including the radionuclide, ground-water chemistry, retardation mechanism, pore/fracture shape and size distribution, and temperature. In addition, if the radionuclides are sufficiently volatile, transport may occur in the vapor phase. Vapor phase transport may be the result of convection and/or diffusion. Retardation of radionuclides in the vapor phase will depend upon partitioning between the gas and liquid phases as well as adsorption sites which are directly available to the vapor phase (i.e., where the surface is not wetted). For fractured media, different transport mechanisms may be important for the fractures and matrix. In this section, we will outline a preliminary "order-of-magnitude" analysis to provide an assessment of which transport mechanisms (i.e., convection, bulk diffusion, thermal diffusion, etc.) may be important in order to assess the possible role of vapor-phase transport. The effect of changing saturation on radionuclide transport in the liquid phase will not be addressed in this report.

The rate at which radionuclides will migrate through porous media in either the gas or liquid phase depends upon:

1. Fluid velocity
2. Percent saturation,
3. Radionuclide concentration,
4. Radionuclide chemical state,
5. Diffusion/dispersion coefficient,
6. Tortuosity
7. Presence of fractures

If the gas and/or liquid velocities are small, diffusional transport of radionuclides may be faster than convective transport. The mass-transfer Peclet number, Pe=vd/D, is an indication of the relative magnitudes of diffusion and convection. For Pe much less than 10^{-2}, convection may be neglected and for Pe greater than 10^{+2}, diffusion may be neglected. Thus, if we know the fluid velocity, v, a characteristic length, d, for the fracture/matrix and the diffusion/dispersion coefficient, D, we can ascertain which transport mechanisms are important [Dullien, 1979]. At the low velocities expected at a repository, D is equal to the diffusivity divided by a tortuosity factor. For fractures, the value of the tortuosity will be close to 1.0. Several different diffusion mechanisms may play a role in gas-phase transport including bulk, Knudsen, and thermal diffusion. Given typical fracture sizes and temperature gradients expected in tuff, bulk diffusion is expected to be the dominant mode.

3.2 Flow/Diffusion Analysis

If convection is the primary transport mode in both phases, an approximate estimate of the relative convective transport rates in the vapor and liquid phases may be obtained from:

$$\alpha_{con} = K_w \ v_g(1-S)R_l/(v_l S R_g) \qquad (9)$$

where α_{con} is the mobility ratio due to convection, R_g and R_l are retardation factors of the gas and liquid, respectively, v_g and v_l are the velocity of the gas and liquid, S is the degree of liquid saturation and K_w is the vapor-liquid distribution coefficient. A preliminary estimate of the ratio, α_{con}/K_w, may be obtained by assuming that the retardation factors, R_g and R_l, are equal and calculating velocity and saturation information. In a similar manner, for very small Peclet number in both the gas and liquid phases, a diffusion mobility ratio may be defined as:

$$\alpha_{dif} = K_w D_g(1-S)R_l/(D_l S R_g) \qquad (10)$$

where α_{dif} is the mobility ratio due to diffusion/dispersion and D_g and D_l are the diffusion/dispersion coefficients for the gas and liquid phase, respectively. If both diffusion and convection are important for a given phase, or if the dominant mechanisms are different for the vapor and liquid phases, simple expressions relating vapor and liquid transport are not available.

The magnitude of the vapor-liquid distribution coefficient, K_w, depends upon the particular radionuclide of interest and its chemical state. Therefore, to accurately calculate K_w values, a wide range of information concerning ground-water conditions (i.e., pH, Eh, concentrations of all major and minor components, etc.) is required. To obtain a first-order approximation, the value of K_w may be calculated by both assuming that the water behaves as an ideal solution and using the pure-component vapor pressure of the radionuclide. Although this assumption could yield an approximate K_w value which may be incorrect by an order of magnitude, this level of accuracy will be sufficient for our bounding calculations. Also, if this assumption is not used, it will be difficult to calculate gas-liquid partitioning coefficients due to the lack of accurate chemical-activity/vapor-pressure data over a range of temperature for many radionuclides of interest. The value of K_w is expected to be a strong function of temperature since both the vapor pressure and chemical state of the species will change. However, this temperature effect is minimized by the general decrease in gas-phase concentrations with increasing temperature. Although calculations have been reported in the literature for the chemical state of various radionuclides in typical NTS tuff ground waters at 293 K [Guzowski, et al., 1983], no information has been reported for higher temperatures.

We have calculated "order-of-magnitude" K_W values by making the following assumptions:

1) The ground water may be treated as pure water.
2) The gas and liquid phases are in thermal equilibrium.
3) The gas phase may be treated as an ideal gas mixture.
4) The liquid may be treated as an ideal, binary solution.

A suite of common compounds were selected such that a wide range of K_W was obtained. These compounds are not all of direct interest in nuclear-waste isolation but they serve to illustrate the behavior of volatile radionuclides for which vapor-phase transport may be important. Table 1 contains K_W values for these compounds at temperatures of 293 K and 373 K. To understand the magnitude of these numbers, the reader must remember that a value of 1.0 corresponds to the radionuclide concentrations in the gas phase and liquid phase being equal. For radionuclides heavier than cesium, vapor-pressure data at these temperatures are not available simply because they are too difficult to measure. Of course for these heavier elements, one would not expect any vapor transport because of these very low vapor pressures and therefore, K_W values are meaningless. For example, extrapolation of high-temperature vapor-pressure data for actinide oxides to 373 K indicates vapor pressures in the range of 10^{-40} to 10^{-30} atm.

TABLE 1. TYPICAL K_W VALUES FOR SELECTED ELEMENTS IN GROUND WATER

	293 K	373 K
Hydrogen[1]	54	75
Oxygen[1]	32	71
Krypton[2]	16	44
Radon[2]	4	15
Iodine[1]	1×10^{-6}	6×10^{-6}
Cesium[1]	2×10^{-9}	5×10^{-8}

Vapor pressure reference:
[1]Lange's Handbook of Chemistry [1979]
[2] IUPAC Solubility Series [1979]

3.3 Flow Simulation

For our preliminary calculations, we have used the TOUGH computer code [Pruess, 1985] to simulate simplified radial two-dimensional and axisymmetric three-dimensional heat canister problems similar to those described by Pruess and Wang [1983]. TOUGH solves the equations for

two-phase flow of air and water in both the gas and liquid phases, and transport of heat in a fully-coupled way. Water and dissolved air are simulated in the liquid phase, and water vapor and air are simulated in the gaseous phase. The governing equations account for gaseous diffusion, Darcy flow, and capillary-pressure effects. Vaporization and condensation of water with latent heat effects and conduction and convection of heat flow are included in the energy balance. Water, air, and rock are assumed to be in thermodynamic equilibrium at all times. The flow domain can include liquid, gas, and two-phase (liquid-gas) regions, indicating that the code can handle both saturated or unsaturated flows problems. This analysis was performed for an equivalent porous medium although data for candidate unsaturated tuff formations [Tien et al., 1985] indicate fractured zones. However, recently Klavetter and Peters [1986] showed that the use of an equivalent porous medium seems adequate for this type of geologic media.

TOUGH solves three nonlinear partial differential equations simultaneously using an integrated finite-difference method. Time stepping is accomplished by a fully-implicit procedure. The resulting nonlinear difference equations are linearized by the Newton-Raphson method. The resulting equations are solved by the Harwell matrix solver which stores only the nonzero elements of a matrix.

We ran an axisymmetric three-dimensional and a radial two-dimensional problem. Several characteristics were similar between the two problems. For both problems, a canister with length of 4.7 m and radius of 0.1715 m is placed at r=0 of either the radial or radial-vertical grid. The waste canister releases energy at an initial rate of 2210 W. This release of energy decays exponentially with time to a rate of 1600 W after 10 years. The rock properties used in the modeling are representative of unsaturated tuff. These include a porosity of 0.12, a rock grain density of 2600 kg/m^3, a permeability of 10^{-15} m^2, a rock-grain thermal conductivity of 2.1 W/m-K, and a rock-grain specific heat of 800 J/kg-K [Tien et al., 1985]. Corey's curves were used to describe the degree of saturation/relative permeability curves. These curves were used as they are the ones considered in the TOUGH code [Pruess, 1986]. More recent empirical data on saturation-relative permeability behavior should be used in the assessment of the repository performance. For this problem, Corey's curves yield the following equations to describe the relative permeabilities:

$$k_{rl} = S^4 \tag{11}$$

and

$$k_{rg} = (1-S^2)\ (1-S)^2 \tag{12}$$

where k_{rl} and k_{rg} are the relative permeability of the liquid and gas, respectively, and S is the degree of liquid saturation. The gas relative permeability curve reproduces the data in Table VI of Travis et al. [1984] fairly well for small degrees of saturation (see Figure 3.1). However, at large degrees of saturation, the gas relative permeability curve underpredicts the Travis et al., [1984] permeability data by an

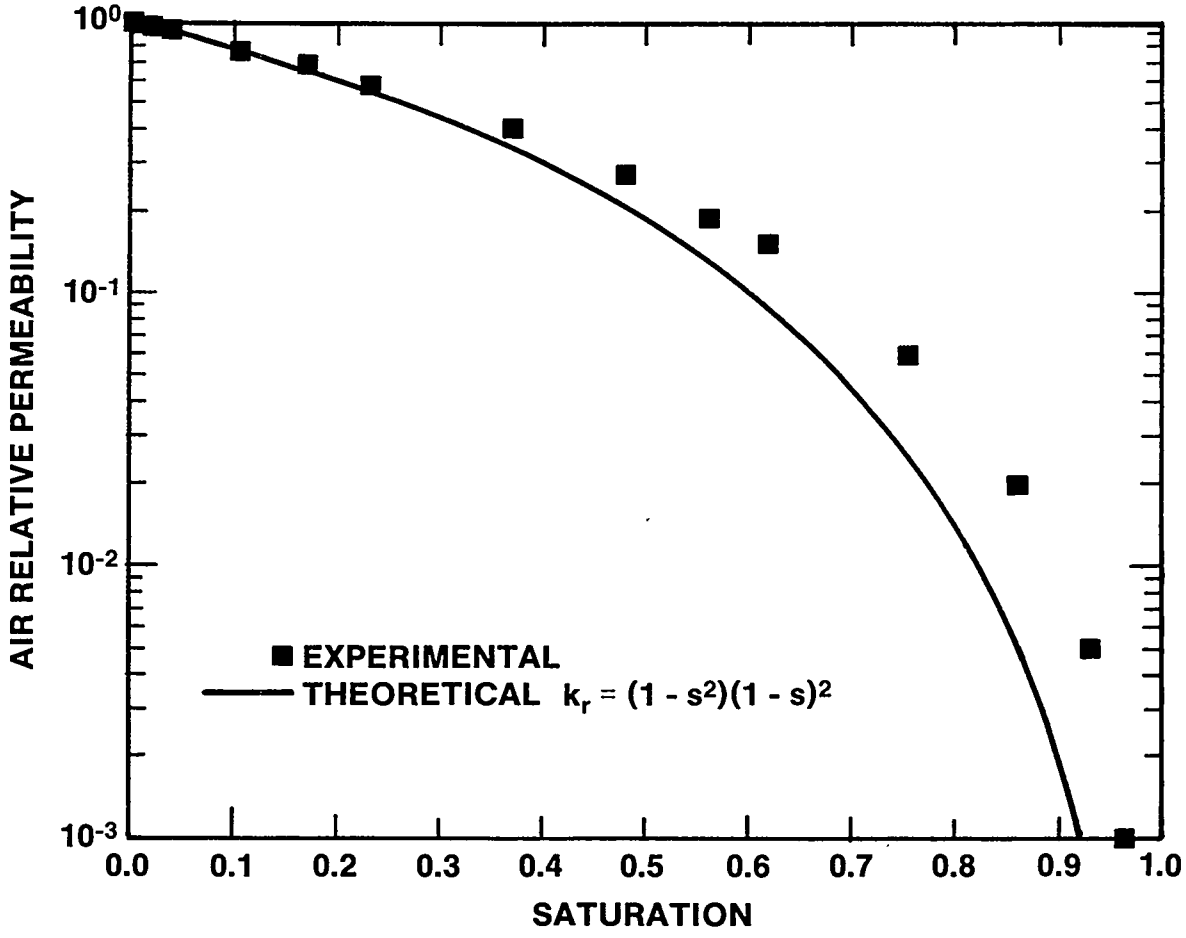

Figure 3.1 Gas Relative Permeability Curve From Equation (12) and Data From Travis et al., [1984].

order of magnitude. The liquid relative permeability curve consistently overestimates the Travis et al., [1984] data by a factor of two for high degrees of saturation and by several orders of magnitude for low degrees of saturation (see Figure 3.2). The capillary pressure versus degree of saturation curve is given by:

$$P_{cap} = -P_o \left[(1-S)/S\right]^{1/\zeta} \qquad (13)$$

where P_{cap} is the capillary pressure and P_o and ζ are constants. For this problem, values of P_o and ζ of 6×10^5 Pa and 0.8, respectively, fit the data provided in Table V of Travis et al. [1984] fairly well (see Figure 3.3). The Travis et al. [1984] data has been used in other studies of unsaturated flow at Yucca Mountain.

3.3a Axisymmetric Three-Dimensional Model

The purpose of the axisymmetric three-dimensional model was to estimate the effects of infiltration on the relative rate of vapor-phase transport to liquid-phase transport. For this simulation, we modeled an area with an outer boundary at a radial distance of 100 m from the canister, an upper boundary, which corresponds to the land surface, at 456 m above the center of the canister, and a lower boundary, which corresponds to the water table at 304 m below the canister center. A schematic of the system analyzed is shown in Figure 3.4.

In the radial direction, there were 15 grid blocks. The canister element had a grid-block width of 0.1715 m. Subsequent grid blocks were expanded at such a rate that the width of one grid block to the width of the preceding grid block (i.e. $\Delta r_i/\Delta r_{i-1}$) was equal to 1.45.

In the vertical direction, 29 grid blocks were used. The top and bottom grid blocks were used to set the boundary conditions for the simulation. Four grid blocks (each of height 1.175 m) were used to represent the canister. In the upward direction from the canister, 12 grid blocks were expanded such that the height of one grid block to the height of the preceding grid block (i.e., $\Delta h_i/\Delta h_{i-1}$) was 1.50. A similar process was used to create 11 grid blocks below the canister. Nodes were placed at the center of the grid block elements.

The following conditions were applied to the boundaries of the modeled area. Zero-flux conditions were applied at both the inner and outer boundaries in the radial direction. At the bottom boundary, we kept the pressure constant at 101,300 Pa (atmospheric pressure), the temperature constant at 293 K, and the degree of liquid saturation constant 1.0, or fully saturated, because of the water table boundary. These boundary conditions allow for the flux of water and heat into the water table but prevent gas from flowing into the water table. At the top boundary, the flux of water was set at 0.1 mm per year in accordance with estimates of vertical flux through the tuffs at Yucca Mountain [Montazer and Wilson, 1984; Weeks and Wilson, 1984]. Additional conditions set at the top

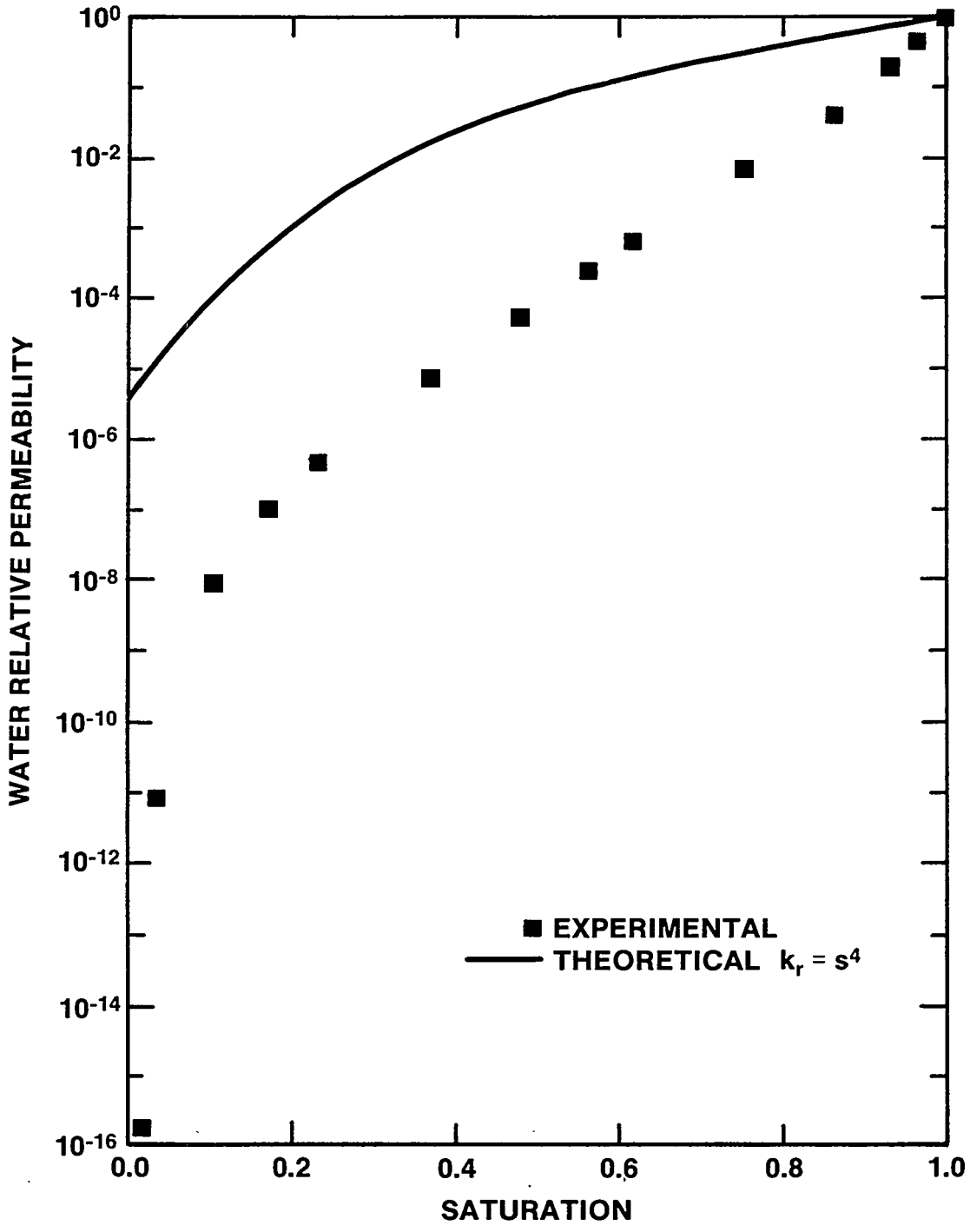

Figure 3.2 Liquid Relative Permeability Curve From Equation (11) and Data From Travis et al., [1984].

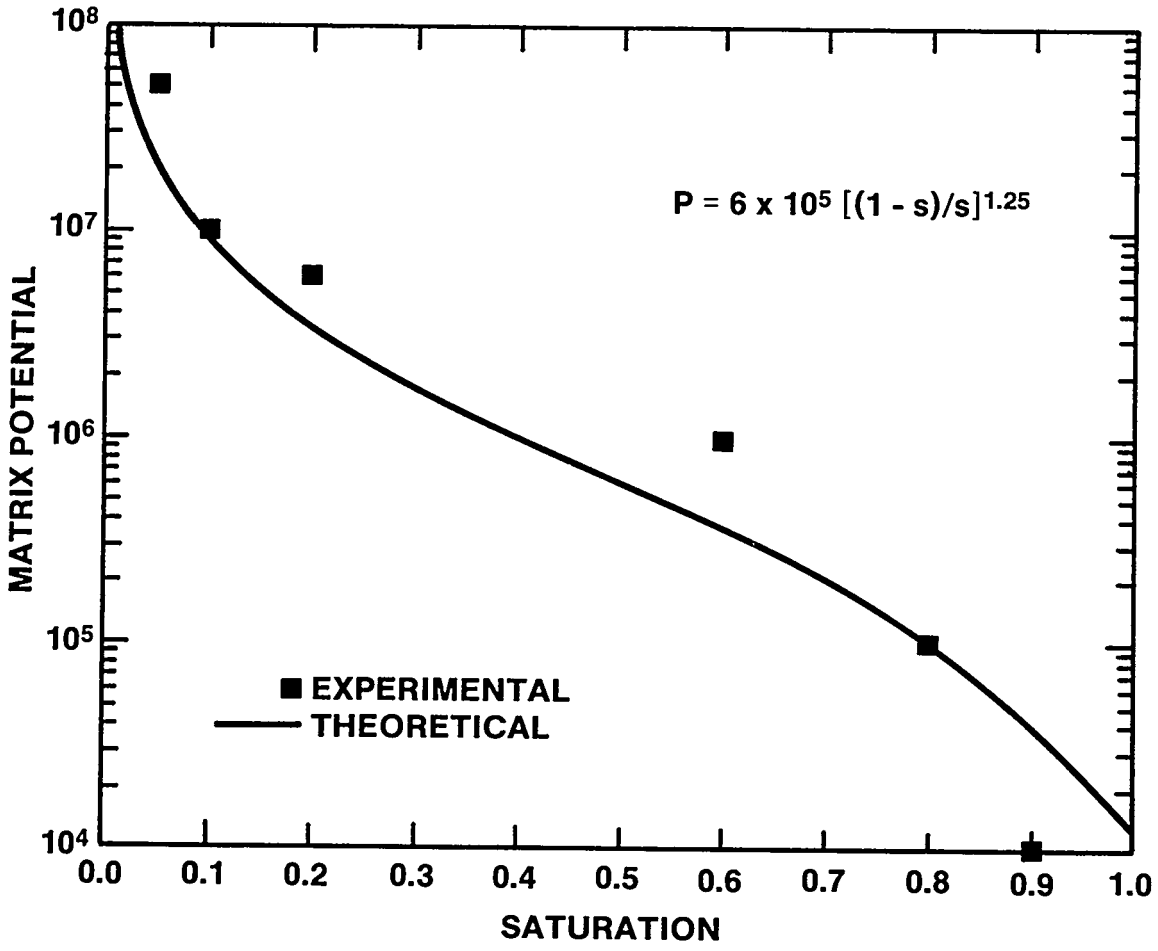

Figure 3.3 Capillary-Pressure Curve From Equation (13) and Data From Travis et al., [1984].

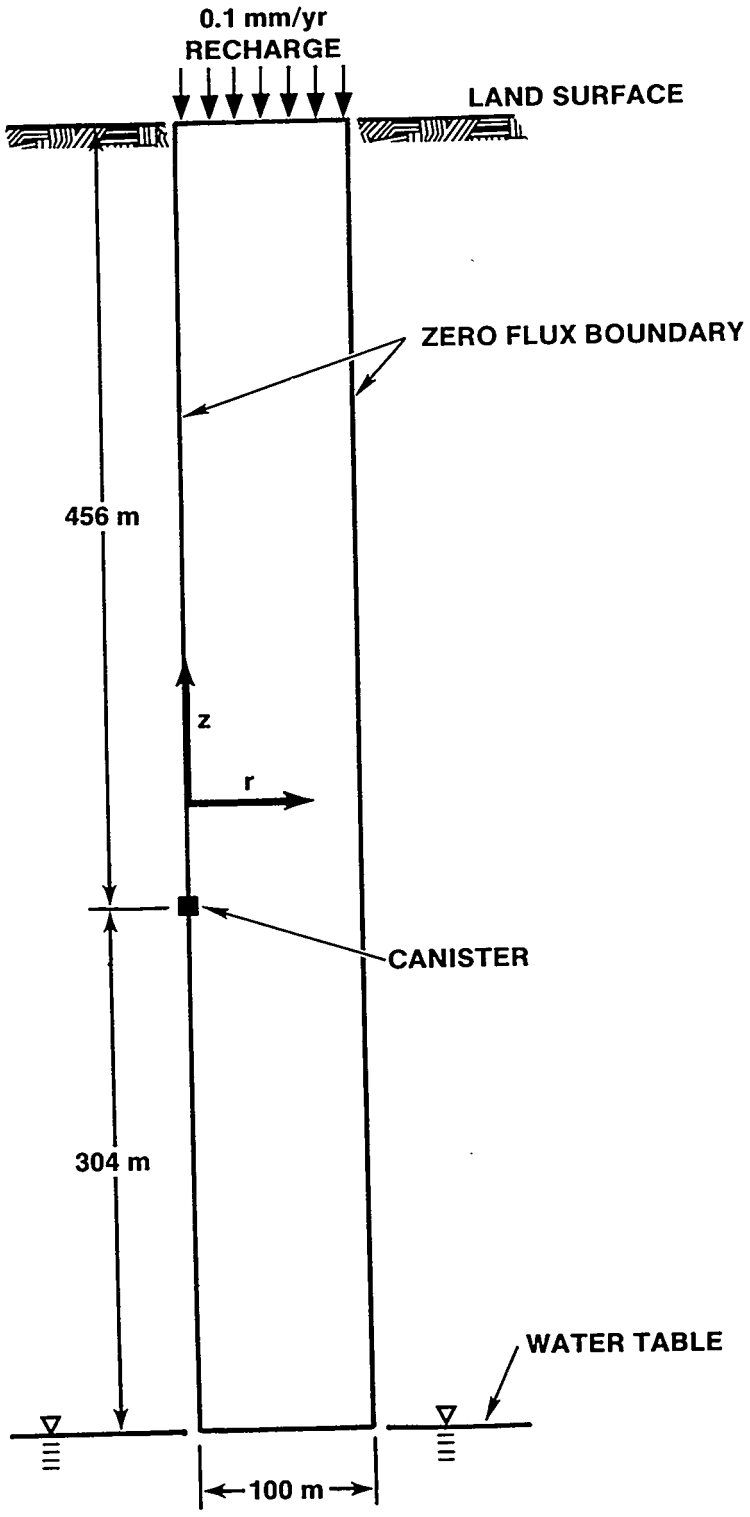

Figure 3.4 Schematic of Axisymmetric Three-dimensional Problem.

boundary include a constant temperature of 293 K, and a constant pressure of 992,765 Pa. These conditions allow for the flux of heat and gas into the atmosphere. The pressure at the top boundary was estimated from modeling conducted to determine the initial conditions.

Initial conditions for pressure and saturation were determined by steady-state modeling of infiltration into a one-dimensional vertical column which used the same grid-block spacing as the vertical grid-block spacing for the three-dimensional case described above. The bottom boundary condition was kept the same as for the three-dimensional simulation and, at the top boundary, liquid was injected at the rate of 0.1 mm per year while gas was allowed to escape to the atmosphere. The output from this simulation consisted of a pressure and degree of saturation profile with respect to depth. These profiles and a constant temperature of 293 K were used as the initial conditions for the three-dimensional modeling.

The degree of saturation calculated from the vertical modeling do not agree very well with those measured at Yucca Mountain. The discrepancy is likely to be caused by the use of a single strata in the analysis. The calculated degrees of saturation range from 1.00 at the water table to 0.24 at the land surface. Measured degrees of saturation at Yucca Mountain typically range between 0.65 and 0.99 but there does not seem to be any significant trend with depth [Tien et al., 1985]. The inconsistencies between the measured and calculated degrees of saturation are probably due to heterogenities of the hydrologic parameters that exist in the physical system but are not accounted for in the model, poor matching between the Travis et al., [1984] relative permeability characteristic curves and the functions used to described them, and an estimate of the recharge rate for which there is a poor degree of confidence.

3.3b Radial Two-Dimensional Model

The purpose of the radial two-dimensional model was to determine if such a model could approximate the temperature, pressure, and saturation effects of the above-described axisymmetric three-dimensional model. If the results of the radial two-dimensional model compared favorably with the results of the axisymmetric three-dimensional model, then we could use two-dimensional models to calculate rate of vapor transport relative to liquid transport. Using a two-dimensional model reduces costs significantly.

For the two-dimensional model, we located our grid on the same horizontal plane as the canister in the above-described three-dimensional model. The radial grid contained 25 grid blocks, each with a height of 4.7 m, which correspond to the height of the canister. The first element, which contained the canister, had a width of 0.1715 m, the canister radius. The second and third elements had widths of 0.5271 and 0.4694 m respectively. Subsequent elements had a width such that the width of one grid block to the width of the preceding grid block (i.e., $\Delta r_i/\Delta r_{i-1}$) equaled 1.17. Nodes were placed at the center of the grid block elements. The radial distance between the center of the canister and the outer boundary was 100 m.

The inner boundary conditions were set so that there was no flux of liquid, vapor, or heat across the boundaries. The outer boundary was kept at a constant temperature, pressure, and degree of saturation.

The initial conditions were based on the steady state modeling results of the one-dimensional vertical model used to set the initial conditions for the three-dimensional runs. We used, for initial conditions, the one-dimensional vertical model predictions along the horizontal plane running through the middle of the canister. Along the horizontal plane opposite the canister, the vertical model predicted a pressure of 97,788 Pa and a degree of saturation of 0.26879. The initial temperature was set at 293 K.

3.4 Flow/Diffusion/Temperature Results

Spatial temperature profiles calculated using the TOUGH code are presented in Figure 3.5 for a time of 3 years and a tuff permeability of 10^{-15} m^2. Included in Figure 3.5 are results for both the two-dimensional and the three-dimensional simulations. The various curves for the three-dimensional simulation correspond to different vertical elevations. The distances are the distance above or below the canister centerline. For any radial position, temperatures at an equal distance above and below the canister are equivalent. This equivalency effect may be negated at longer times by buoyancy effects. The time period of three years was selected since the canister wall temperature had approached the maximum temperature corresponding to the particular set of repository conditions used in the simulation (i.e., heat loading, permeability, porosity, saturation, etc.). Also, radial temperature profiles at/near the canister centerline elevation (z=0.6 m for the three-dimensional case) approach the linear change with log of radius which corresponds to the steady-state, analytical solution for conductive heat transfer in cylindrical coordinates. Two findings of the three-dimensional versus two-dimensional simulations are interesting. Near the canister centerline, the two-dimensional and three-dimensional simulations agree quite well. This is somewhat surprising since much of the heat transfer is due to convection associated with the complex flow field around the canister, the so-called "heat pipe effect." The other significant finding is that the temperature drops sharply at relatively small vertical distances (< 10 m) from the canister. This second finding may be caused by the effect of most of the heat being directed radially out of the side of the canister rather than through the top or bottom.

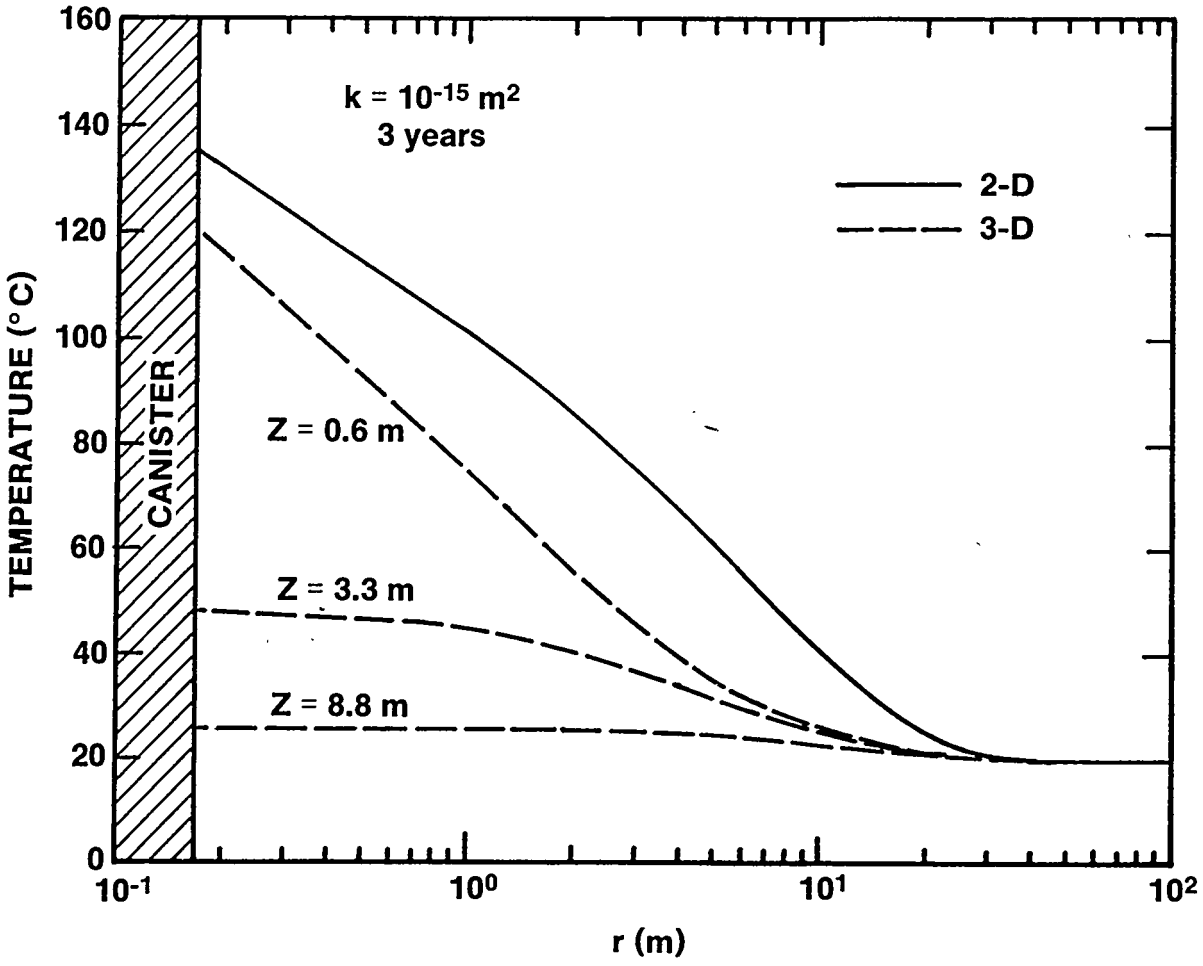

Figure 3.5 Radial Temperature Distributions at Various Elevations After 3 Years.

The large spatial variation in tuff temperature at a given time has several implications for possible vapor-phase transport. Since radionuclide vapor pressure is a function of temperature, the vapor pressure, and hence, K_w, may vary by an order of magnitude (see Table 1) for a given time at different locations in tuff. One would expect that vapor transport will be greatest at the points of highest temperature (i.e. near the canister). This would be the result of higher K_w, reduced saturation, and the large vapor velocities associated with the transport of heat away from the canister. Also, this variation in temperature will change the ground-water chemistry. However, little information concerning the chemical state of radionuclides in tuff ground water at elevated temperature is available.

From our calculations, the ratio of the vapor phase volumetric flow rate to that in the liquid phase α_{con}/K_w, is obtained. The radial variation of this ratio is plotted in Figure 3.6 for a time of 3 years and a permeability of 10^{-15} m^2. There is good qualitative agreement between the two-dimensional and three-dimensional simulations but as with the temperature-field results, the two-dimensional simulation tends to overpredict the results of the three-dimensional simulation. Near the waste container, negative values of the mobility ratio are noted. This is the result of liquid ground water flowing towards the container, the liquid vaporizing and the vapor being forced away from the canister by a net pressure gradient. At small vertical distances from the canister, this heat-pipe effect rapidly disappears. Near the outer boundary of the simulated region, the magnitude of the mobility factor becomes significant. This is the result of either the boundary condition or the initial degree of saturation. Because of the low initial degree of saturation, the relative permeability of the medium with respect to the gas is much higher than the permeability to the liquid. At distances far from the canister, the degree of saturation does not change very much. Near the canister, the degree of saturation changes rapidly due to the vaporization of water. Thus, at large distances from the canister, the change in capillary pressure does not significantly affect the water pressure and the pressure gradients in the two phases are approximately equal. The high relative gas permeability coupled with the low gas viscosity compared to that of the liquid indicates that the rate of vapor transport is much higher than the rate of liquid transport at large distances from the canister and for similar gas and liquid pressure gradients.

In addition to the mobility factor, a knowledge of the flow rates of each phase is important since the mobility ratio gives only relative information about which phase may be important. Plotted in Figure 3.7 are the product of the radial velocity (m/s) and gas saturation ((1-S) for gas phase) at the canister centerline. Positive flow rates (i.e., towards the canister) are indicated by solid lines and negative flow rates are indicated by dotted lines. As discussed previously, liquid water in the vicinity of the canister flows towards the canister and is

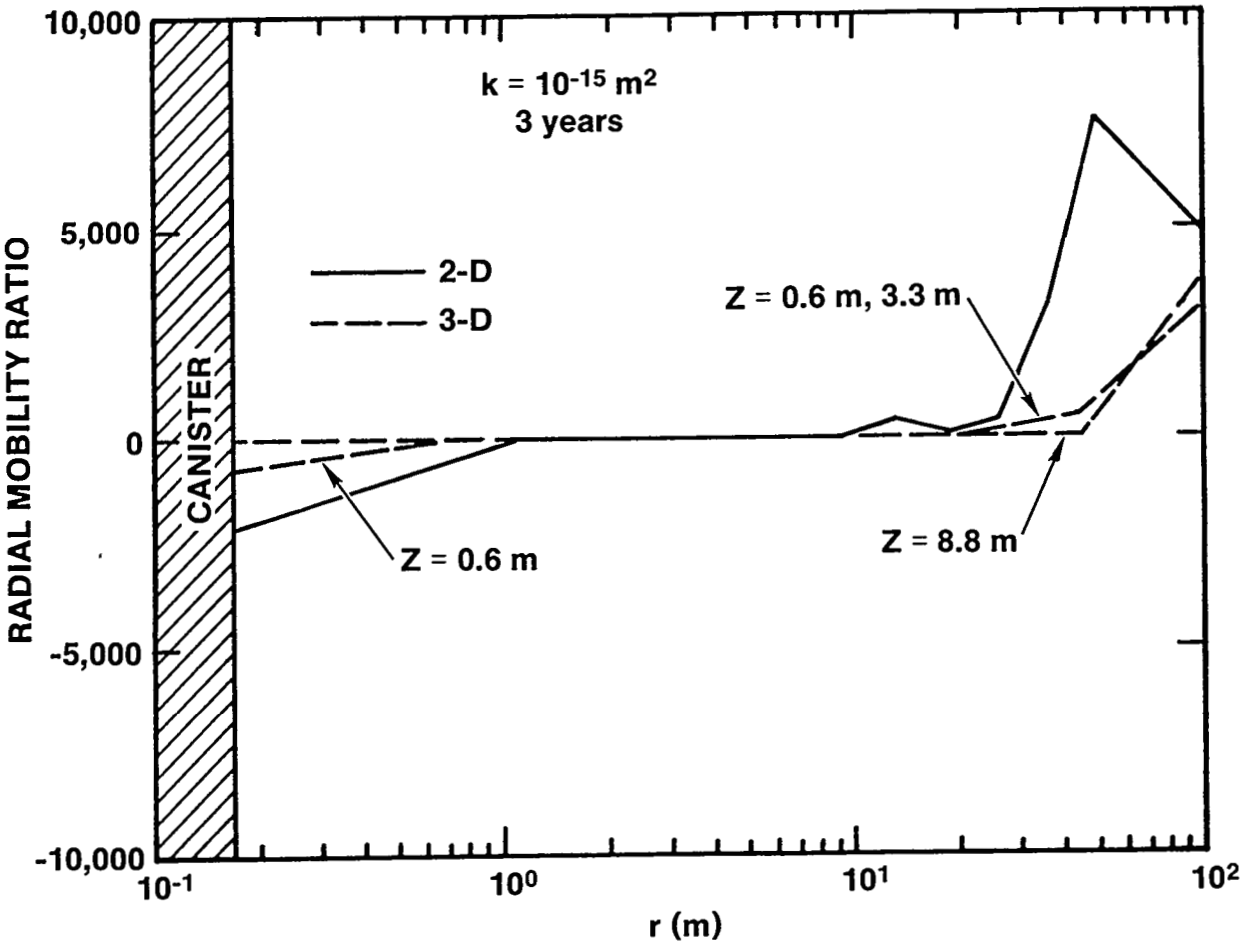

Figure 3.6 Radial Mobility Factor as a Function of Radial and Vertical Position After 3 Years.

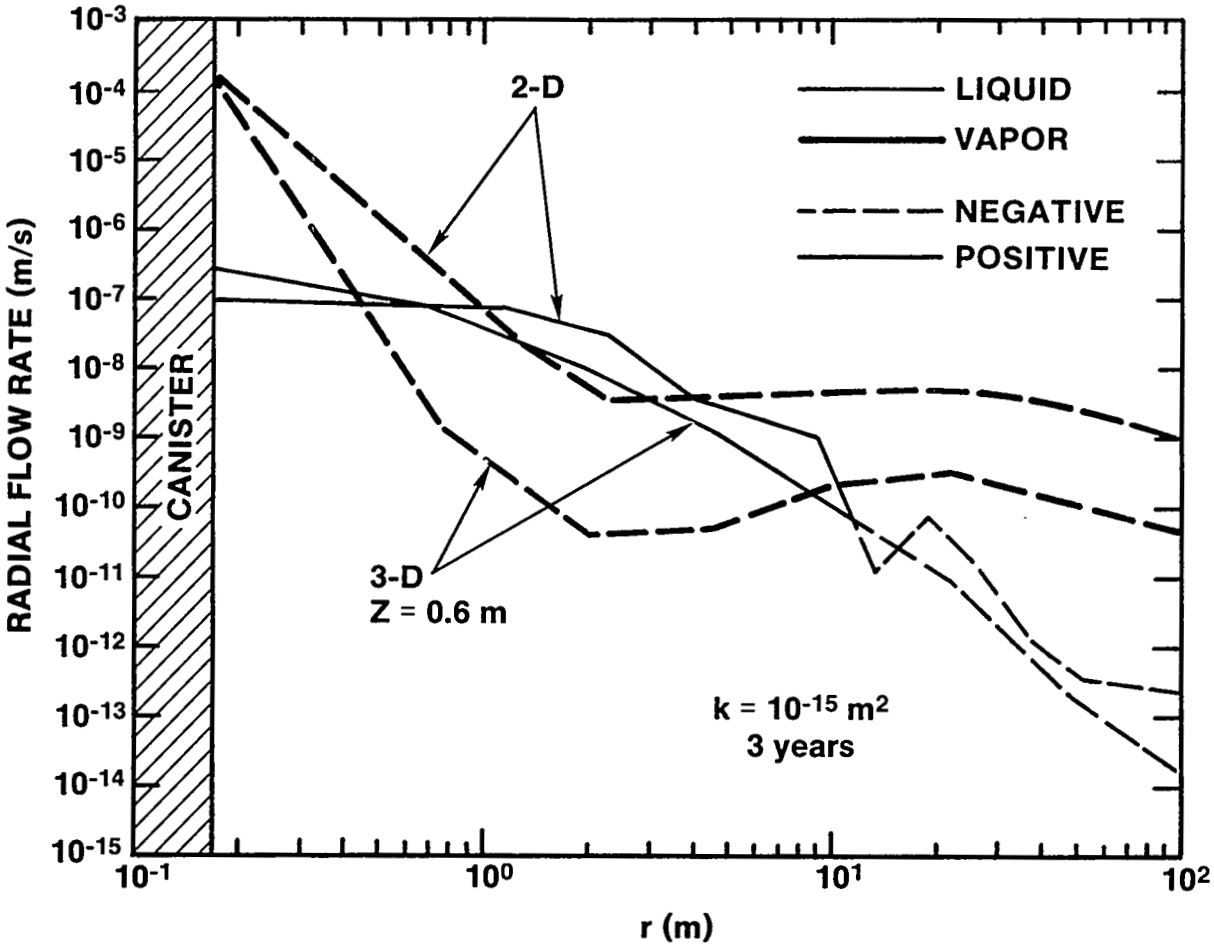

Figure 3.7 Radial Flow Rates as a Function of Radial and Vertical Position After 3 Years.

vaporized. The vapor then flows away from the canister at a relatively high flow rate. However, this effect only extends for several meters away from the canister. For longer times, the heat-pipe effect will extend further from the canister but velocities will decrease due to the lower heat loading. The agreement between the two- and three-dimensional simulations is remarkable considering that the vapor and liquid flow rates vary over ten orders of magnitude. The relatively large values of the mobility factor near the outer boundary seem unimportant when the 10^{-10} m/s gas velocity is considered.

The vertical mobility factor at various elevations in the simulated region as a function of radial position is plotted in Figure 3.8. Except in the immediate vicinity of the canister, r<1 m, vertical mobility of the vapor phase may be neglected. The complex circulation pattern near the waste canister is illustrated by both positive and negative values of the mobility factor at the same radial position but different elevations. However, this large scale vapor circulation is damped out within 10 meters measured vertically from the canister centerline. The spatial distributions of liquid vertical flow rate (liquid velocity x S) and vapor flow rate (gas velocity x (1-S)) are presented in Figure 3.9. Outside of several meters from the canister, liquid flow rates are substantially greater than the gas flow rates. At a distance of 10 meters above or below the canister, liquid flow rates are greater than gas flow rates for all radial positions.

If the maximum velocities reported above are used in conjunction with a range of reasonable values for the diffusivity and fracture spacing, the mass-transfer Peclet number (Pe) may be calculated. The maximum value of Pe in either the gas or liquid phases is on the order of 100 while the minimum value is on the order of 10^{-9}. Therefore, the mass transfer mechanism may be dominated by convection in the immediate vicinity of the canister but diffusion will dominate at greater distances. As time increases, the possible importance of convective transport will disappear.

To calculate values of the diffusion mobility ratio, α_{diff}, we use Equation (10) with the assumption that $R_g=R_l$. The gas and liquid diffusivity may be estimated using the Chapman-Enskog and Wilke-Chang theories [Reid, et al., 1977]. Depending upon the species considered, the value of α_{con}/K_w will be in the range of 100 to 10,000 at 293 K. This suggests that for a preliminary estimate of the importance of vapor-phase transport for a particular radionuclide, one could thus use the product of 1000 and the value of K_w for that species to obtain the ratio of vapor-phase to liquid-phase transport.

Calculations have only been performed over the first 3 years of the repository lifetime since we are performing a preliminary, "worst-case"

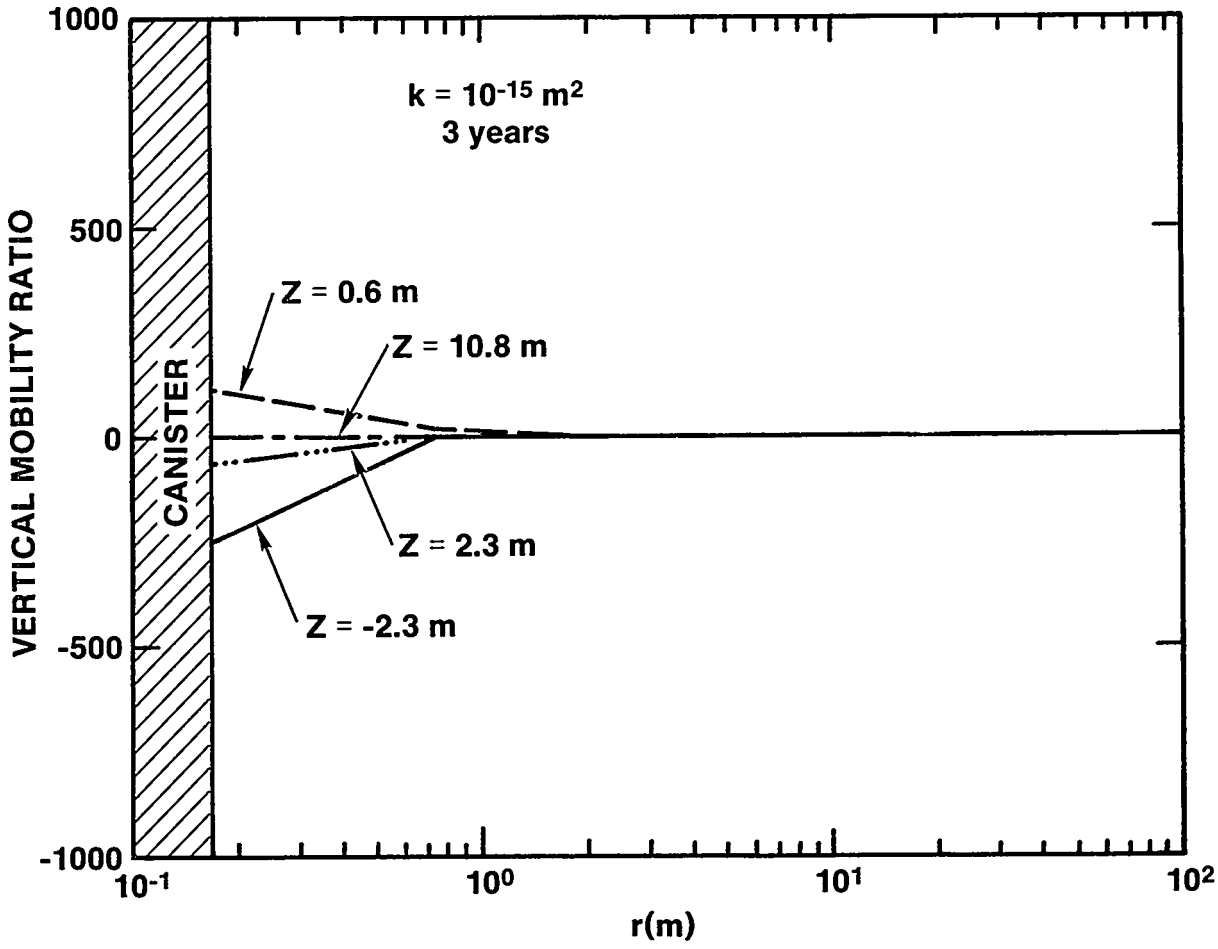

Figure 3.8 Vertical Mobility Factor as a Function of Radial and Vertical Position After 3 Years.

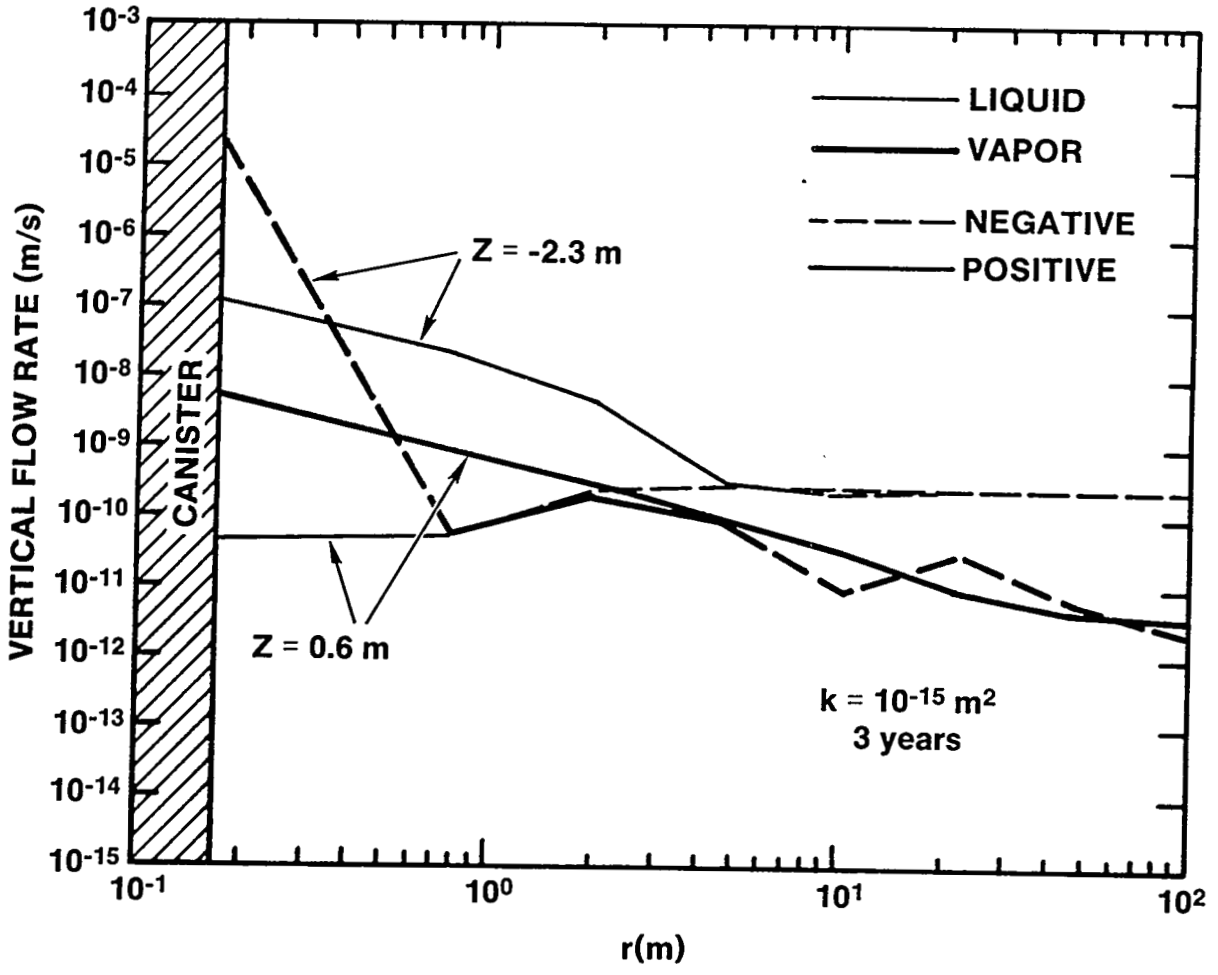

Figure 3.9 Vertical Flow Rates as a Function of Radial and Vertical Position After 3 Years.

analysis of the possibility of transport in the vapor phase. As time increases past 3 years, it is not expected that conditions will become more favorable for vapor-phase transport. Of course, this time cutoff is dependent on the simulation conditions used. After 3 years, the maximum temperature and minimum saturation appear to have reached a plateau. Both of these conditions favor the increased importance of transport in the vapor phase as compared to the liquid phase. Therefore, the possible importance of vapor-phase transport for a particular radionuclide and repository conditions will be greatest within the first 3 years of the repository lifetime.

3.5 Far-Field Bounding Calculations

Although the results of the previous section certainly indicate that vapor phase will not be important in the vicinity of the canister for radionuclides heavier than radon, the large values of α_{con}/K_w near the outer boundary of the simulated region are cause for concern. The initial assumption that the greatest possibility of vapor transport will be in the near field as a result of high temperature and low saturation may be in error. To assess the possibility of vapor-phase transport in the far field, we have conducted calculations which serve to provide an upper bound for the mobility factor. By using a simplified analysis, the cost of detailed long-term simulations is avoided at the expense of a less accurate answer. However, since our simplified analysis will result in an upper bound for the mobility factor, we will still be able to make effective and conservative conclusions concerning vapor-phase transport.

3.5a Radial Bounding Calculations

The radial Darcy velocity for the gas/vapor phase in unsaturated flow is described by [Dullien, 1979] as

$$q_g = -k\, k_{rg}/\mu_g\, [\nabla P_g - \rho_g\, g] \qquad (14)$$

The analogous expression for the liquid phase is

$$q_l = -\, k\, k_{rl}/\mu_l\, [\nabla P_l - \rho_l\, g] \qquad (15)$$

The pressure gradients for the liquid and gas streams are related to the capillary pressure gradient by

$$\nabla P_l - \nabla P_g = \nabla P_c \qquad (16)$$

In the radial direction, far removed from the canister, the spatial change in saturation will be small. This implies that the liquid and gas pressure gradients are equivalent. For radial transport, we may also assume that density (i.e., buoyancy) effects are negligible. If we

assume that retardation for the two phases is equal, the mobility factor, by definition, is q_g/q_l. Therefore, rearranging Equations 14 through 16, α_{con}/K_w may be approximated by:

$$\alpha_{con}/K_w = k_{rg}\mu_l/(\mu_g k_{rl}) \qquad (17)$$

The mobility factor may be calculated as a function of the degree of saturation using Equation (17) and Equation (11) and (12), which relate relative permeability to saturation.

The upper bound for the mobility factor has been calculated as a function of saturation and is presented in Figure 3.10. The temperature is assumed to be 293 K and pressure is 1 atmosphere. The large increases in the mobility factor as saturation decreases is readily evident. As discussed before, this is the result of the highly nonlinear relationships between liquid and gas relative permeability and saturation as described in Figure 3.1 and 3.2. It is interesting to note that our results from this simple calculation scheme are within 20% of the results of our three-dimensional calculation for spatial locations far removed from the canister. We should point out that the results of our bounding calculations slightly over-predict the vapor phase transport contribution (i.e., more conservative).

3.5b Vertical Bounding Calculations

In a similar manner to the radial calculations, we simplify Equations (14) and (15) by assuming that one force is dominant. In this, we assume that gravity effects will dominate gas and liquid flow. Therefore, the pressure gradient terms may be neglected. We should point out this assumption is not rigorous but will result in an upper bound on vapor phase mobility. Assuming that retardation in the two phases is equal, Equations (14) and (15) may be combined to yield the following expression for the mobility factor:

$$\alpha_{con}/K_w = k_{rg}\rho_g\mu_e/(k_{rl}\rho_e\mu_g) \qquad (18)$$

Assuming that the formation temperature is 293 K and that the pressure is atmospheric, the mobility factor may be calculated. Our calculations of the mobility factor as a function of saturation are presented in Figure 3.11. The plot parallels the results of the radial bounding calculations for radial transport but at a much lower level. This is expected since examination of Equations (17) and (18) indicates that the two expressions are identical except for the inclusion of the ratio of gas to liquid density (which will always be much less than one).

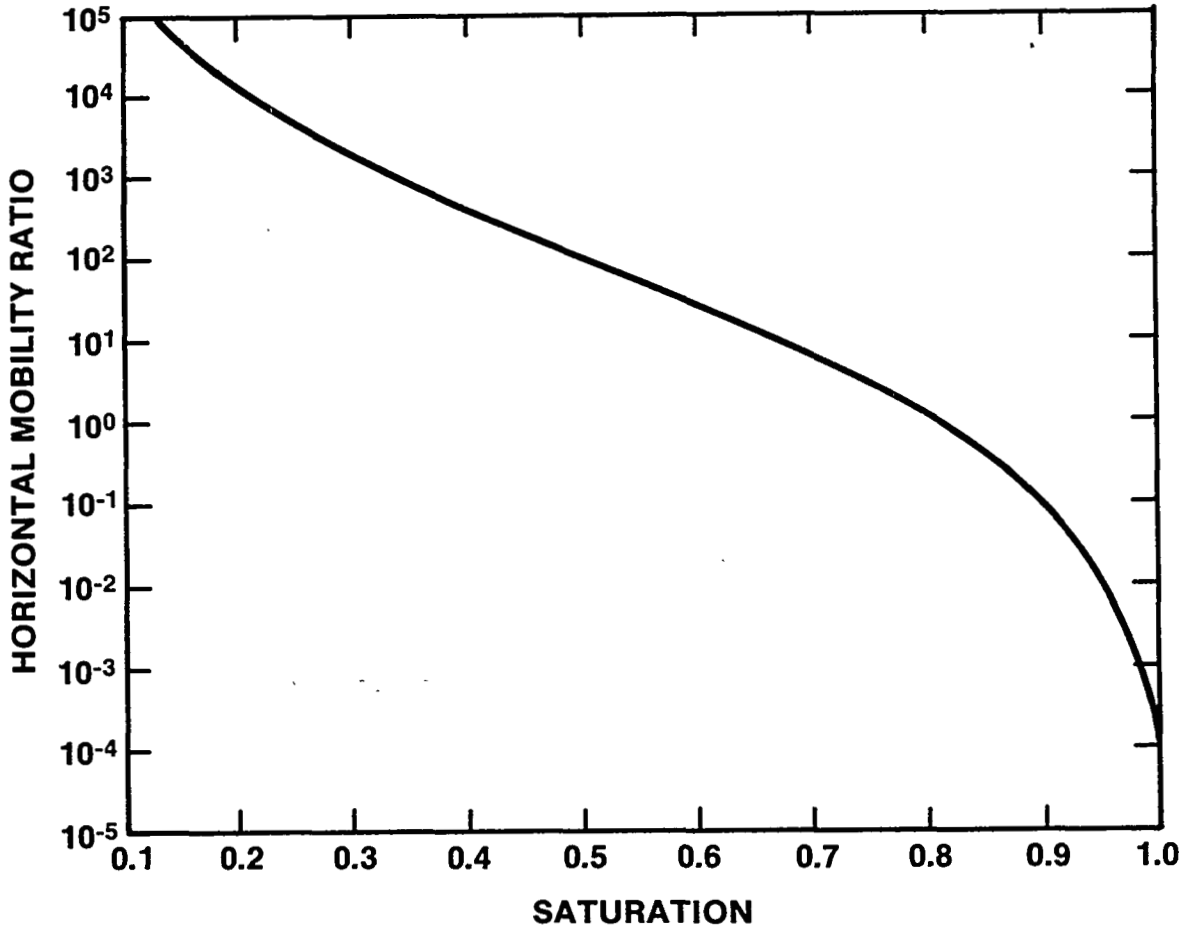

Figure 3.10 Far-Field Radial Mobility Factor as a Function of Liquid Saturation.

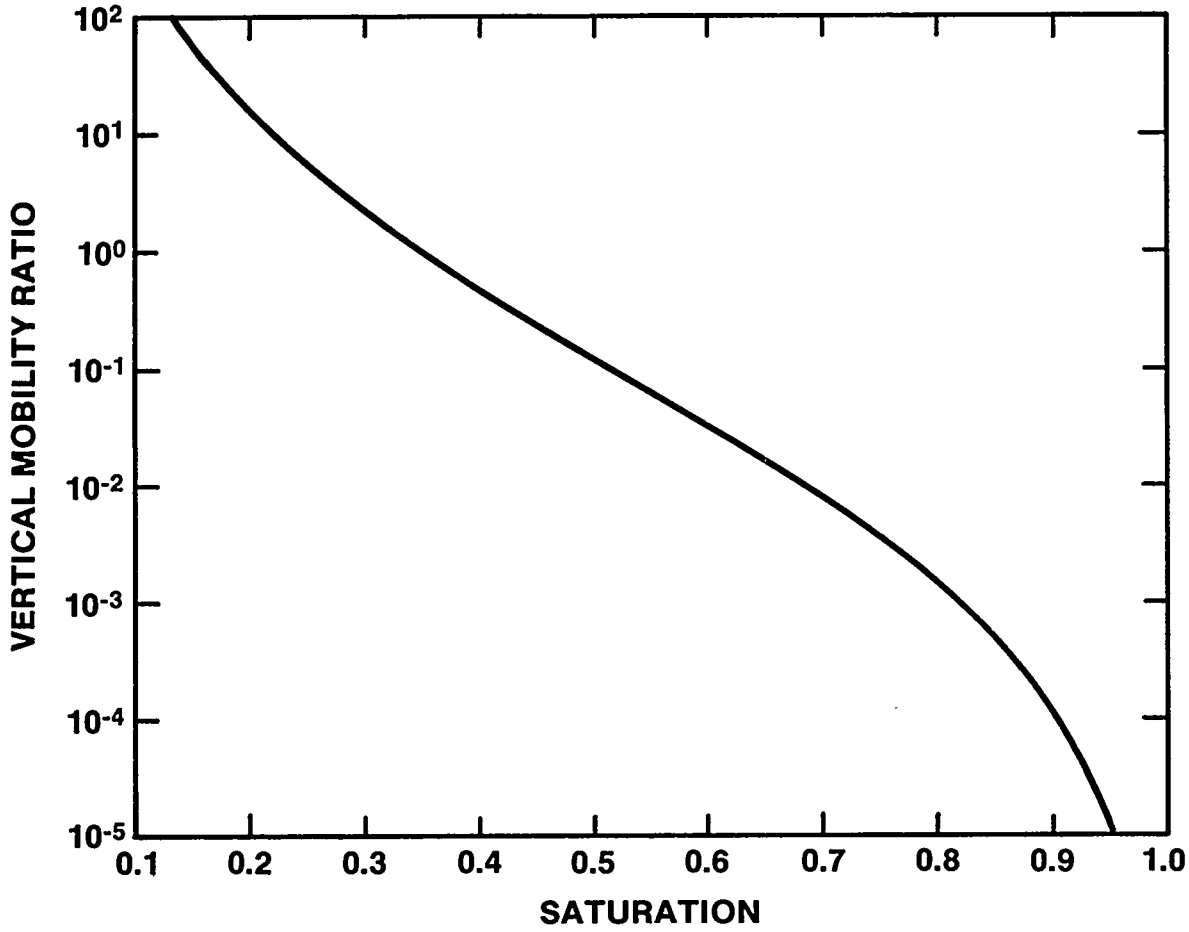

Figure 3.11 Far-Field Vertical Mobility Factor as a Function of Liquid Saturation.

4. FUTURE WORK

In this work, we have provided conservative bounding calculations related to the possibility of radionuclide transport in the unsaturated zone as either an aerosol or a volatile species. However, we have not addressed the question of what effect the unsaturated zone will have on the retardation of radionuclides in the liquid phase. The important question of how the retardation factor changes with saturation can only be answered after detailed information concerning both the pore structure of tuff and the interaction of tuff with water/water vapor is obtained. When that information is available, conservative first-order approximation of the retardation/saturation relationship may be formulated.

5. CONCLUSIONS

The possibility of radionuclide transport in the vapor phase due to either the formation/migration of aerosols or as volatile species has been investigated via a series of bounding calculations. Based upon an analysis of the various steps necessary in an aerosol formation scenario, we have identified a straightforward set of calculations to address the possibility of aerosol transport in the unsaturated zone. From the results of a suite of calculations which cover the range of possible repository conditions, it is clear that aerosol formation will not occur and the concept of radionuclide transport as an aerosol may be safely neglected.

The TOUGH code has been used to calculate spatial and temporal distributions of liquid and gas velocity, saturation, and temperature for typical tuff formation properties. Both radial two-dimensional and axisymmetric three-dimensional simulations were undertaken. The calculated distributions have been used to determine the relative transport rates due to convection in the gas phase as compared to the liquid phase. Except for the immediate region of the canister (i.e., within several meters,) transport in the liquid phase will dominate for all radionuclides except radon and lighter (more volatile) species. In the immediate canister vicinity, vapor-phase transport of iodine may also be important. Although several simulations are not sufficient to state the conditions when vapor-phase transport is not important, we provide a simple technique which may be combined with flow calculations to assess vapor transport for specific repository conditions. An analogous mobility ratio when diffusion dominates radionuclide transport (i.e., small Peclet number) has also been calculated.

Bounding calculations for vapor-phase transport in the far field have also been conducted. The radial and vertical mobility factors have been calculated as a function of saturation in a manner which provides a conservative estimate of vapor-phase transport. Maximum values of α_{con} are on the order of 10^6 K_w for the lowest reasonable formation saturation. Vertical mobility factors are approximately three orders of magnitude less than radial mobility factors at a given saturation. The results of these bounding calculations agreed quite well with our axisymmetric three-dimensional simulations for regions far removed from the canister.

Based upon our calculations for flow and heat transfer in both the near-field and far-field, it is clear that vapor-phase transport will not be important for radionuclides such as cesium and heavier species. Vapor transport for iodine may play a role in the overall release scenario depending on the particular repository conditions.

6. NOMENCLATURE

C = Concentration(mole/m^3).

D = Diffusion/dispersion coefficient (m^2/s).

D_{AB} = Diffusivity of dissolved air in water (m^2/s).

d = Characteristic fracture spacing(m).

g = gravity (m/s^2).

K_w = Vapor-liquid distribution coefficient.

k = Permeability(m^2).

k_r = Relative permeability(m^2).

L = Liquid film thickness(m).

m = $\sqrt{s/D}$

P = Pressure(Pa).

Pe = Peclet number.

q = Darcy velocity(m/s).

R = Retardation factor.

r_b = Air bubble radius(m).

S = Saturation.

S' = Fractional supersaturation.

s = Laplace transform variable.

t = Time(s).

t_d = Time constant for changing air solubility(s).

t^* = Dimensionless constant, $L^2/t_d D_{AB}$.

v = Fluid velocity(m/s).

x = Spatial variable(m).

α = Mobility ratio.

β = C_f/C_o.

γ = $C-C_o$.

Δh = Height of a grid block used in numerical modeling(m).

Δr = Width of a grid block used in numerical modeling(m).

λ_n = Eigenvalues, $(2n+1)\pi/2$.

ρ = Density(kg/m^3).

n = Dimensionless distance.

σ = Surface tension(N/m).

Θ = Dimensionless concentration, $(C-C_o)/C_o$.

6. NOMENCLATURE (cont.)

Θ = Fourier transformed concentration, defined in Equation (3).

τ = Dimensionless time, $D_{AB}t/L^2$

μ = Dynamic viscosity(Pa-s).

υ = $1/t_d$.

ζ = Constant in Equation (13).

Subscripts

b = Bubble

cap = Capillary.

con = Convection.

dif = Diffusion.

f = Final condition.

g = Gas phase.

i = Index.

l = Liquid phase.

o = Initial condition.

7. REFERENCES

Abramowitz, M. and I.A. Stegun, HANDBOOK OF MATHEMATICAL FUNCTIONS, Dover Publications Inc., New York, New York, 1965.

Carslaw, H.S. and J.C. Jaeger, CONDUCTION OF HEAT IN SOLIDS, 2nd Edition, Oxford University Press, Oxford, Britain, 1959.

Danckwerts, P. V., GAS-LIQUID REACTIONS, McGraw-Hill, New York, NY, 1970.

Dullien, F.A.L., POROUS MEDIA - FLUID TRANSPORT AND PORE STRUCTURE, Academic Press, New York, NY, 1979.

Green, R.T. and D.D. Evans, Radionuclide Transport as a Vapor through Unsaturated Fractured Rock - A Preliminary Assessment, NRC-04-81-224 Contract Report, 1983.

Guzowski, R.V., F.B. Nimick, M.D. Siegel, N.C. Finley, Repository Site Data Report for Tuff: Yucca Mountain, Nevada, NUREG/CR-2937, SAND82-2105, Sandia National Laboratories, Albuquerque, NM, 1983.

Hidy, G.M., AEROSOLS: AN INDUSTRIAL AND ENVIRONMENTAL SCIENCE, Academic Press, New York, NY, 1984.

Hsu, Y.Y., and R.W. Graham., TRANSPORT PROCESSES IN BOILING AND TWO-PHASE SYSTEMS, McGraw-Hill, New York, New York, 1976.

Klavetter, E.A., and R.R. Peters, Fluid Flow in Fractured Rock Mass, SAND85-0855, Sandia National Laboratories, Albuquerque, NM, 1986.

IUPAC SOLUBILITY SERIES-Volume 2, Pergamon Press, London, 1979.

LANGE'S HANDBOOK OF CHEMISTRY, McGraw Hill, 12 Ed., New York, NY, 1979.

Montazer, P. and W.E., Wilson, Conceptual Hydrologic Model of Flow in the Unsaturated Zone, Yucca Mountain, Nevada. Water-Resources-Investigations Report 84-4345, U.S. Geological Survey, 1984.

Ogard, A.E., K.Wolfsberg, and D.T. Vaniman, Research and Development Related to the Nevada Nuclear Waste Storage Investigations, April 1-June 30, 1983, LA-9846-PR, Los Alamos National Laboratory, Los Alamos, NM, 1983.

Ozisik, M.N., BOUNDARY VALUE PROBLEMS OF HEAT CONDUCTION, International Textbook Company, 1968.

Pruess, K., TOUGH User's Guide, LBL-20700, Lawrence Berkeley Laboratories, Berkeley, CA, to be published 1986.

Pruess, K. and J.S.Y. Wang, TOUGH - A Numerical Model for Nonisothermal Unsaturated Flow to Study Waste Container Heating Effects, LBL-16946, Lawrence Berkeley Laboratory, Berkeley, CA 1983.

Reid, R.C., J.M. Prausnitz, and T.K. Sherwood, THE PROPERTIES OF GASES AND LIQUIDS, 3rd Ed., McGraw-Hill, New York, NY, 1977.

Satterfield, C.N., MASS TRANSFER IN HETEROGENOUS CATALYSIS, MIT Press, Cambridge, MA, 1970.

Tien, P., M.D. Siegel, C.D. Updegraff, K.K. Wahi, and R.V. Guzowski, Repository Site Data Report for Unsaturated Tuff, Yucca Mountain, Nevada, NUREG/CR-4110, SAND84-2668, Sandia National Laboratories, Albuquerque, NM, 1985.

Tomaides, M. and K.T. Whitby, Generation of Aerosols by Bursting of Single Bubbles, FINE PARTICLES: AEROSOL GENERATION, MEASUREMENT, SAMPLING AND ANALYSIS, Academic Press, New York, NY 1976.

Travis, B.V., S.W. Dodson, H.E. Nuttall, T.L. Cook, and R.S. Rundberg, Preliminary Estimates of Water Flow and Radionuclide Transport in Yucca Mountain, LA-UR-84-40, Los Alamos National Laboratory, Los Alamos, NM, 1984.

Weeks, E.P. and W.E. Wilson, Preliminary Evaluation of Hydrologic Properties of Cores of Unsaturated Tuff, Test Well USW H-1, Yucca Mountain, Nevada, Water-Resources Investigations Report 84-4193, U.S. Geological Survey, 1984.

APPENDIX

SHORT-TIME ASYMPTOTIC SOLUTIONS FOR DIFFUSION EQUATION

The series solution for $\theta(\eta,\tau)$ given in equation (6) converges very slowly for small values of τ requiring the evaluation of a large number of terms in the expansion. In this appendix we outline two approaches leading to short-time asymptotic solutions that do not exhibit convergence problems. For longer times the series solution for $\theta(\eta,\tau)$ is recommended.

The first approach presented here solves the following partial differential equation

$$\frac{\partial \gamma}{\partial t} = D\frac{\partial^2 \gamma}{\partial x^2} \tag{A-1}$$

subject to the following initial and boundary conditions

$$\left.\begin{aligned} &\gamma(x,0) = 0 \\ &\frac{\partial \gamma}{\partial x}(0,t) = 0 \\ &\gamma(L,t) = (C_f - C_0)\,[1-e^{-\nu t}] \end{aligned}\right\} \tag{A-2}$$

where $\gamma = C - C_0$ and $\nu = 1/t_d$. Letting $\bar{\gamma}(x,s)$ be the Laplace transform of $\gamma(x,t)$ and s the Laplace-transform variable results in

$$\bar{\gamma}(x,s) = (C_f - C_0)\,[1/s + 1/(\nu+s)]\,\cosh(mx) / \cosh(mL) \tag{A-3}$$

where $m = \sqrt{s/D}$. Small values of time correspond to large values of s. Thus, in the limit of time approaching zero, cosh(mL) can be expanded for large values of mL. We shall also express cosh(mx) in terms of its two exponential functions such that

$$\cosh(mx)/\cosh(mL) \approx \sum_{n=0}^{\infty} (-1)^n \sum_{j=1}^{2} \exp\{-m\,[(2n+1)L + (-1)^j x]\} \tag{A-4}$$

Equations (A-3) and (A-4) suggest that the inverse of the Laplace transform must be obtained for functions of the general form

$$\frac{\exp(-my)}{s} \quad \text{and} \quad \frac{\exp(-my)}{(\nu+s)}$$

which are listed in Appendix V of Carslaw and Jaeger [1959], for example, as

$$\mathcal{L}^{-1}[e^{-my}/s] = \operatorname{erfc}(y/\sqrt{4Dt}) \tag{A-5}$$

and

$$\left.\begin{aligned}\mathcal{L}^{-1}[e^{-my}/(\nu+s)] = e^{-\nu t}/2 \Big\{ & e^{-iy/\sqrt{\nu/D}} \operatorname{erfc}(y/\sqrt{4Dt} - i\sqrt{\nu t}) \\ & + \\ & e^{iy/\sqrt{\nu/D}} \operatorname{erfc}(y/\sqrt{4Dt} + i\sqrt{\nu t}) \Big\}\end{aligned}\right\} \tag{A-6}$$

where $\mathcal{L}^{-1}$ denotes the inverse Laplace transform and $i = \sqrt{-1}$. Equation (A-6) can be simplified using equations (7.1.3) and (7.1.4) in Abramowitz and Stegun [1965] and integrating by parts via Hermite integration [see equation (25.4.46) in Abramowitz and Stegun]. The inverse Laplace transform of equation (A-3) then becomes

$$\left.\begin{aligned}\gamma(x,t) = (C_f - C_0)\Bigg\{ & \sum_{n=0}^{\infty} (-1)^n \sum_{j=1}^{2} \left[\operatorname{erfc} \frac{(2n+1)L + (-1)^j x}{\sqrt{4Dt}} \right] \\ & - 2/\pi \sum_{n=0}^{\infty} (-1)^n \sum_{j=1}^{2} \exp\left[\frac{-[(2n+1)L + (-1)^j x]^2}{4Dt} \right] \times \\ & \int_{-\infty}^{\infty} \tan^{-1}\left[\frac{(\sqrt{\nu t} + u)\sqrt{4Dt}}{[(2n+1)L + (-1)^j x]} \right] u e^{-u^2} \, du \Bigg\}\end{aligned}\right\} \tag{A-7}$$

For the very short times of interest in this analysis, only terms corresponding to n=0 and j=1,2 need be retained in equation (A-7).

In the second approach we solved the partial differential equation

$$\frac{\partial \theta}{\partial \tau} = \frac{\partial^2 \theta}{\partial \eta^2} \tag{A-8}$$

subject to the initial and boundary conditions

$$\left.\begin{aligned} &\theta(\eta,0) = 0 \\ &\frac{\partial\theta}{\partial\eta}(0,\tau) = 0 \\ &\theta(1,\tau) = K = \text{constant} \end{aligned}\right\} \qquad \text{(A-9)}$$

Letting $\bar{\theta}(\eta,s)$ be the Laplace transform of $\theta(\eta,\tau)$ we get

$$\bar{\theta}(\eta,s) = \frac{K\cosh(\sqrt{s}\,\eta)}{s\cosh(\sqrt{s})} \qquad \text{(A-10)}$$

Once again, since we are only interested in short-time solutions ($\tau \to 0$), s becomes very large. In this case we use the approximation

$$\cosh(\sqrt{s}) \approx e^{\sqrt{s}} / 2.$$

Then equation (A-10) becomes

$$\bar{\theta}(\eta,s) = K\left[\frac{e^{-(1-\eta)\sqrt{s}}}{s} + \frac{e^{-(1+\eta)\sqrt{s}}}{s}\right] \qquad \text{(A-11)}$$

which can be readily inverted to give

$$\theta(\eta,\tau) = K\left\{\text{erfc}[(1-\eta)/(2\sqrt{\tau})] + \text{erfc}[(1+\eta)/(2\sqrt{\tau})]\right\} \qquad \text{(A-12)}$$

Since we are interested in the solution for

$$K = (1-\beta)\,[e^{-t^*\tau} - 1] \qquad \text{(A-13)}$$

we applied Duhamel's theorem to obtain

$$\theta(\eta,\tau) = -t^*(1-\beta)\int_0^\tau e^{-t^*u}\left\{\text{erfc}[(1-\eta)/(2\sqrt{\tau-u})] + \text{erfc}[(1+\eta)/(2\sqrt{\tau-u})]\right\}\,du. \qquad \text{(A-14)}$$

Equations (A-7) and (A-15) should be identical when only the leading term in the summation over n is retained in the former and the proper variables transformations have been performed.

DISTRIBUTION

U.S. Government Printing Office
Receiving Branch (Attn: NRC Stock)
8610 Cherry Lane
Laurel, MD 20707
305 copies for RW

U.S. Nuclear Regulatory Commission (5)
Office of Nuclear Regulatory Research
Washington, DC 20555
Attn: G. Arlotto
G. F. Birchard
D. L. Chery, Jr.
F. A. Costanzi
M. Cullingford

U.S. Nuclear Regulatory Commission (5)
Office of Nuclear Regulatory Research
Washington, DC 20555
Attn: R. Grill
R. Kornasiewicz
L. Kovach
T. J. McMartin
M. B. McNeil

U.S. Nuclear Regulatory Commission (5)
Office of Nuclear Regulatory Research
Washington, DC 20555
Attn: T. J. Nicholson
W. Ott
J. Philip
D. Ross
L. Shao

U.S. Nuclear Regulatory Commission (10)
Office of Nuclear Regulatory Research
Washington, DC 20555
Attn: J. D. Randall

U.S. Nuclear Regulatory Commission (1)
Office of Nuclear Regulatory Research
Washington, DC 20555
Attn: Resource Management Branch

U.S. Nuclear Regulatory Commission (5)
Office of Nuclear Material Safety and Safeguards
Washington, DC 20555
Attn: M. J. Bell
J. Bradbury
D. Brooks
P. Brooks
R. E. Browning

U.S. Nuclear Regulatory Commission (5)
Office of Nuclear Material Safety and Safeguards
Washington, DC 20555
Attn: J. T. Buckley
R. C. Carter
Document Control Center, DWM
K. C. Chang
R. B. Codell

U.S. Nuclear Regulatory Commission (5)
Office of Nuclear Material Safety and Safeguards
Washington, DC 20555
Attn: N. Coleman
S. Coplan
L. Deering
A. Elzeftawy
D. J. Fehringer

U.S. Nuclear Regulatory Commission (5)
Office of Nuclear Material Safety and Safeguards
Washington, DC 20555
Attn: M. Fliegle
G. N. Gnugnoli
D. Goode
J. Greeves
D. Gupta

U.S. Nuclear Regulatory Commission (5)
Office of Nuclear Material Safety and Safeguards
Washington, DC 20555
Attn: J. Hunt
A. K. Ibrahim
K. C. Jackson
T. Johnson
P. S. Justus

U.S. Nuclear Regulatory Commission (5)
Office of Nuclear Material Safety and Safeguards
Washington, DC 20555
Attn: W. Kelly
M. R. Knapp
M. Nataraja
S. Neuder
J. J. Peshel

U.S. Nuclear Regulatory Commission (5)
Office of Nuclear Material Safety and Safeguards
Washington, DC 20555
Attn: C. H. Peterson
C. L. Pittiglio
J. Pohle
G. W. Roles
J. A. Shaffner

Office of Nuclear Material Safety and Safeguards (5)
Washington, DC 20555
Attn: R. S. Starmer
S. Symkowski
A. Titinsky
M. Tokar
J. Voglewede

Office of Nuclear Material Safety and Safeguards (3)
Washington, DC 20555
Attn: M. F. Weber
E. A. Wisk
D. Widmayer

Lawrence Berkeley Laboratory (5)
One Cyclotron Road
Berkeley, CA 94720
Attn: J. Apps
C. Carnahan
M. Lippmann
J. Long
T. N. Narasimhan

Lawrence Berkeley Laboratory (5)
One Cyclotron Road
Berkeley, CA 94720
Attn: S. Phillips
K. Pruess
C. Radke
C. F. Tsang
J. Wang

Lawrence Berkeley Laboratory (2)
One Cyclotron Road
Berkeley, CA 94720
Attn: P. A. Witherspoon
H. Wollenberg

Battelle Columbus Laboratories (3)
505 King Street
Columbus, OH 43201
Attn: A. Markworth
S. Nicolosi
D. Stahl

Battelle Memorial Institute (2)
505 King Street
Columbus, OH 43201
Attn: P. L. Cloke
T. Verma

Dept. of Hydrology and Water Resources (3)
University of Arizona
Tucson, AZ 85721
Attn: D. D. Evans
S. P. Neuman
E. S. Simpson

Ralph Parsons Laboratory (3)
Dept. of Civil Engineering
Massachusetts Institute of Technology
Cambridge, MA 02130
Attn: R. Bras
L. Gelhar
D. McLauglin

Adrian Brown
10294 Hayden Pass
Littleton, CO 80125

E. J. Davis
Dept. of Chemical Engineering
BF-10
University of Washington
Seatle, WA 98195

J. K. Daemen
Dept. of Mining and Geological Engineering
University of Arizona
Tucson, AZ 85721

J. I. Drever
Dept. of Geology
University of Wyoming
Laramie, WY 82071

H. H. Einstein
Massachusetts Institute of Technology
Room 1-330
Cambridge, MA 02130

N. A. Eisenberg
Office of Civilian Radioactive Waste Management
U.S. Department of Energy
1000 Independence Avenue
Washington, DC 20585

R. E. Ewing
Dept. of Mathematics
University of Wyoming
Laramie, WY 82071

P. Fenske
Dester Research Institute
University of Nevada
Reno, NV 89507

A. L. Gutjahr
Dept. Mathematics
New Mexico Institute of Mining and Technology
Socorro, NM 87801

C. Hung
Mail Stop ANR-460
U.S. Environmental Protection Agency
401 M Street SW
Washington, DC 20460

C. Kraeger-Rovey
2927 W. 36th Avenue
Denver, CO 80211

F. A. Kulacki
Office of the Dean
College of Engineering
Colorado State University
Ft. Collins, Co 80523

D. Langmuir
Dept. Chemistry and Geochemistry
Colorado School of Mines
Golden, CO 80401

A. E. Van Luik
Battelle Pacific Northwest Laboratories
Richland, WA 99352

L. C. Manning
Finger Lakes Hydro
812 East Lake Road
Penn Yan, NY 14527

G. de Marsily
Ecole des Mines de Paris
35, Rue Saint-Honore
77305 Fontainebleau
FRANCE

J. McCray
Nuclear Fuel Cycle Research Program
University of Arizona
Tucson, AZ 85721

C. McKee
In-Situ Inc.
209 Grand Avenue
Laramie, WY 82070

D. Norton
Dept. Geosciences
University of Arizona
Tucson, AZ 85721

I. Randall
I & T Associates
6329 Tamar Drive
Columbia, MD 21045

P. A. Rechard
Western Water Consultants
P.O. Box 4128
Laramie, WY 82070

D. M. Smith (5)
Dept. Chemical and Nuclear Engineering
University of New Mexico
Albuquerque, NM 87131

T. L. Sniff
Waste, Water & Land, Inc.
1311 South College Avenue
Fort Collins, CO 80524

A. Star
A. S. Associates
29 Clay Street
Dansville, NY 14437

D. B. Stephens & Assoc.
P.O. Box 740
Socorro, NM 87801

K. E. Torrance
Sibley School of Mechanical and Aerospace Engineering
Upson and Grumman Halls
Cornell University
Ithaca, NY 14850

S. C. Way
In-Situ Inc.
209 Grand Avenue
Laramie, WY 82070

R. Williams
Williams and Associates Inc.
P.O. Box 48
Viola, ID 83872

L. A. Zaremba
The Aerospace Corporation
Suite 400
955 L'Enhant Plaza, SW
Washington, DC 20024

Sandia National Laboratories

1511 R. Dykhuizen
1511 R. Eaton
3141 S. A. Landerberger (5)
3151 W. L. Garner
6312 R. R. Peters
6400 A. W. Snyder
6430 N. R. Ortiz
6431 R. M. Cranwell
6431 E. J. Bonano (25)
6431 P. A. Davis
6431 E. L. Emerson
6431 R. V. Guzowski
6431 C. P. Harlan
6431 R. L. Hunter
6431 R. Ostmeyer
6431 J. S. Philbin
6431 R. P. Rechard
6431 L. R. Shipers
6431 M. D. Siegel
6431 C. D. Updegraff
6431 K. Wahi
6431 G. F. Wilkinson

NRC FORM 336 (2-84) NRCM 1102, 3201, 3202

U.S. NUCLEAR REGULATORY COMMISSION

BIBLIOGRAPHIC DATA SHEET

SEE INSTRUCTIONS ON THE REVERSE

1 REPORT NUMBER (Assigned by TIDC and Vol No., if any)
NUREG/CR-4693
SAND86-1598

2. TITLE AND SUBTITLE
Assessment of Radionuclide Vapor-phase Transport in Unsaturated Tuff

3 LEAVE BLANK

4 DATE REPORT COMPLETED
MONTH: September YEAR: 1986

5 AUTHOR(S)
D. M. Smith, C. D. Updegraff, E. J. Bonano, and J. D. Randall

6 DATE REPORT ISSUED
MONTH: November YEAR: 1986

7. PERFORMING ORGANIZATION NAME AND MAILING ADDRESS (Include Zip Code)
Sandia National Laboratories
Albuquerque, NM 87185

8 PROJECT/TASK/WORK UNIT NUMBER

9 FIN OR GRANT NUMBER
FIN A-1266

10 SPONSORING ORGANIZATION NAME AND MAILING ADDRESS (Include Zip Code)
Waste Management Branch
Division of Engineering Safety
Office of Nuclear Regulatory Research
U.S. Nuclear Regulatory Commission
Washington, D.C. 20555

11a TYPE OF REPORT
Final

b PERIOD COVERED (Inclusive dates)

12 SUPPLEMENTARY NOTES

13 ABSTRACT (200 words or less)

This report describes bounding calculations performed to investigate the possibility of radionuclide migration in a vapor phase associated with the emplacement of a high-level waste canister in unsaturated tuff formations. Two potential radionuclide transport mechanisms in the vapor phase were examined: aerosol migration and convection/diffusion of volatile species. The former may have significant impact on the release of radionuclides to the accessible environment as the concentration in the aerosols will be equal to that in the ground water. A conservative analysis of air diffusion in a stagnant liquid film indicated that for all expected repository conditions, aerosol formation is not possible. The migration of volatile species was examined both in the vicinity of a waste canister and outside the thermally-disturbed zone. Two-dimensional (radial) and three-dimensional (radial-vertical) coupled heat transfer-gas flow-liquid flow simulations were performed using the TOUGH computer code. The gas flow rate relative to the liquid flow rate predicted from the simulations allowed calculations of mobility ratios due to convection which led to the conclusion that, except for the immediate region near the canister, transport in the liquid phase will be dominant for radionuclides heavier than radon. Near the waste canister, iodine transport may also be important in the vapor phase. Bounding calculations for vertical mobility ratios were carried out as a function of saturation. These calculations are conservative and agree well with the two-dimensional simulations. Based on this analysis, it is clear that vapor-phase transport will not be important for radionuclides such as cesium and heavier species. Vapor transport for iodine may play a role in the overall release scenario depending on the particular repository conditions.

14 DOCUMENT ANALYSIS - a KEYWORDS/DESCRIPTORS

radionuclide transport
vapor-phase transport
aerosols
volatile species
unsaturated media
unsaturated tuff
waste isolation
coupled heat/flow modeling

b IDENTIFIERS/OPEN-ENDED TERMS

15 AVAILABILITY STATEMENT
Unlimited

16 SECURITY CLASSIFICATION
(This page) Unclassified
(This report) Unclassified

17 NUMBER OF PAGES

18 PRICE

☆ U.S. GOVERNMENT PRINTING OFFICE: 1986—773-049/41023